volume on days 9 (before L-OHP treatment) after tumor cell inoculation.

2.10. Statistical analysis

Differences between PEG-liposomes and TF–PEG-liposomes were compared with unpaired Student's *t*-test.

3. Results

3.1. Cytotoxicity of L-OHP encapsulated TF–PEG-liposomes

L-OHP was encapsulated within Bare-, PEG- or TF–PEG-liposomes, all measuring about 180 nm in diameter. The amounts of encapsulated L-OHP within the Bare-, PEG- and TF–PEG-liposomes measured by MIP-MS were 12.3, 19.2 and 14.8 μg/mg liposomal lipid, respectively. We initially assessed the cytotoxicity of these liposomes against Colon 26 cells, which overexpress TF receptors, *in vitro*. Both L-OHP in solution and encapsulated within all three types of liposomes were cytotoxic against Colon 26 cells in a dose-dependent manner (Fig. 1). The ED_{50} values of L-OHP in solution and encapsulated within Bare-, PEG- and TF–PEG-liposomes were 2, 60, 18, and 8 μg/ml for Colon 26 cells, respectively. The L-OHP encapsulated within TF–PEG-liposomes was the most cytotoxic among the three types of the liposomes. In addition, we examined whether the cytotoxicity of L-OHP encapsulated within TF–PEG-liposomes was due to uptake of the liposomes via TF receptor into Colon 26 cells. When liposome uptake via TF receptors was inhibited by adding an excess of TF into medium, the cytotoxicity of L-OHP encapsulated within TF–PEG-liposomes was decreased (Fig. 1). On the other hand, blocking TF receptors did not influence the cytotoxicity of L-OHP encapsulated within PEG-liposomes. These results indicated that TF–PEG-liposomes were internalized into Colon 26 cells via TF receptor-mediated endocytosis and delivered L-OHP into the cytoplasm.

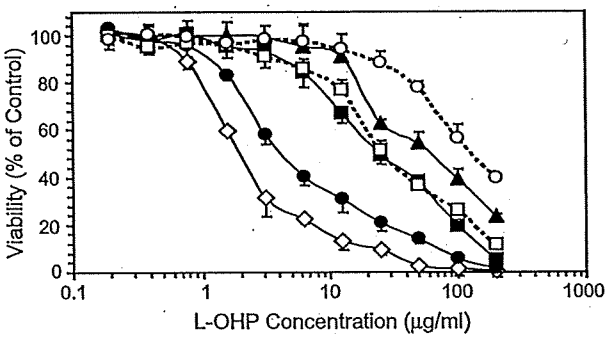

Fig. 1. Cytotoxicity of L-OHP in solution and liposomal L-OHP against Colon 26 cells. Cells were incubated with L-OHP in solution (open diamonds) or encapsulated within Bare- (solid triangles), PEG- (solid squares) or TF–PEG-liposomes (solid circles) without TF, or with PEG- (open squares) or TF–PEG-liposomes (open circles) with TF for 4 h 37 °C under 5% CO_2. Thereafter, cells were washed and incubated with fresh medium for 2 days at 37 °C in 5% CO_2. Cell growth was assayed using WST-1 assay. Maximal cell growth (100%) was obtained by incubating cells without L-OHP. Data are shown as means and standard deviation ($n=5$).

3.2. Biodistribution of L-OHP encapsulated within TF–PEG-liposomes in mice bearing tumors

Liposomes with encapsulated L-OHP were injected i.v. into mice bearing Colon 26 tumors and L-OHP distribution was evaluated. Fig. 2A shows the time course of plasma clearance after the i.v. injection of L-OHP in solution and liposomal L-OHP. The L-OHP in solution was rapidly cleared from the blood circulation whereas the circulation of L-OHP encapsulated within liposomes was increased. The blood concentrations of L-OHP encapsulated within PEG- and TF–PEG-liposomes were much higher than that of L-OHP encapsulated within Bare-liposomes. We also assessed the biodistribution of L-OHP in solution and of L-OHP encapsulated within various liposomes at 6 h after i.v. injection (Fig. 2B). The results showed that very little L-OHP was distributed to the major tissues in mice. In contrast, the distribution of L-OHP encapsulated in PEG- and TF–PEG-liposomes to the liver and spleen differed, but far less of both was distributed to these tissues compared with Bare-liposomes. These results indicated that the PEG layer prolonged the systemic circulation of liposomes after i.v. injection. Thus, the conjugation of TF to the PEG terminal did not alter the RES uptake of PEG-liposomes, presumably because TF is a blood glycoprotein. Furthermore, PEG chains occupying the liposome surface played a role in the prolonged circulation of TF–PEG-liposomes.

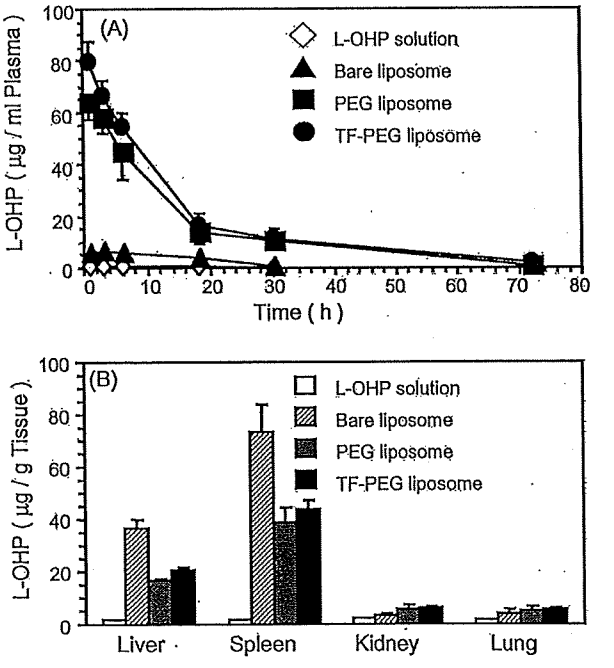

Fig. 2. Plasma clearance (A) and biodistribution (B) of L-OHP solution or liposomal L-OHP in Colon 26-bearing mice. (A) L-OHP in solution or encapsulated within Bare-, PEG- or TF–PEG-liposomes (L-OHP: 5 mg/kg) was injected via tail veins of Colon 26-bearing mice. At various times thereafter, blood samples were collected using glass capillaries from veins of fundus oculi. Plasma L-OHP levels were measured by MIP-MS. (B) L-OHP in solution or encapsulated within Bare-, PEG- or TF–PEG-liposomes (L-OHP: 5 mg/kg) was injected via tail veins of Colon 26-bearing mice. Six hours later, mice were sacrificed and liver, spleen, kidneys and lungs were collected. Concentrations of L-OHP in tissue samples were measured by MIP-MS. Data are shown as means and standard deviation ($n=3$).

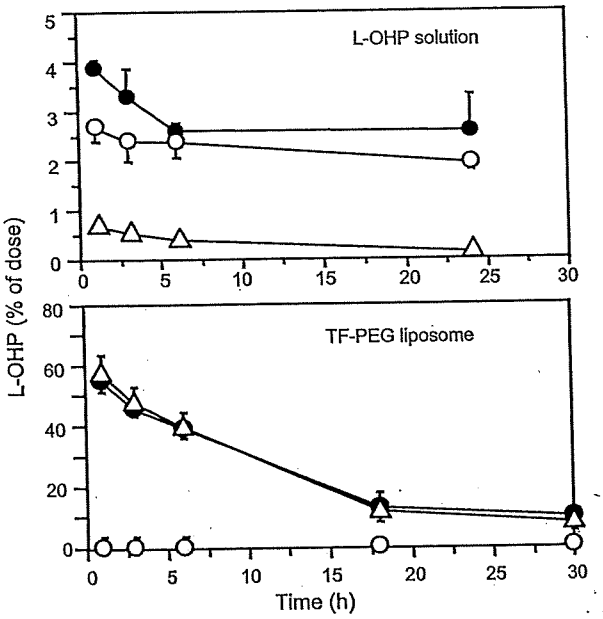

Fig. 3. Partitioning of L-OHP into the erythrocytes in whole blood as a function of time after injecting L-OHP in solution or in TF–PEG-liposomes into tail veins of Colon 26-bearing mice. Concentrations of L-OHP were measured at various time points in whole blood (solid circle), plasma (open triangle) and erythrocyte fraction (open circle). Data are presented as the percentage of the total injected dose for each sample. Data are shown as means and standard deviation ($n=3$).

When L-OHP in solution was injected, the total L-OHP concentration in whole blood was much lower than that of L-OHP in TF–PEG-liposomes, and most of L-OHP in whole blood was taken up by erythrocytes (Fig. 3). In contrast, little L-OHP was distributed to erythrocytes in whole blood when L-OHP encapsulated in TF–PEG-liposomes was injected (Fig. 3). The degree of L-OHP partitioning to erythrocytes remarkably differed between the solution and TF–PEG-liposomes, since the latter were stable in the blood circulation and little L-OHP was released from the liposomes.

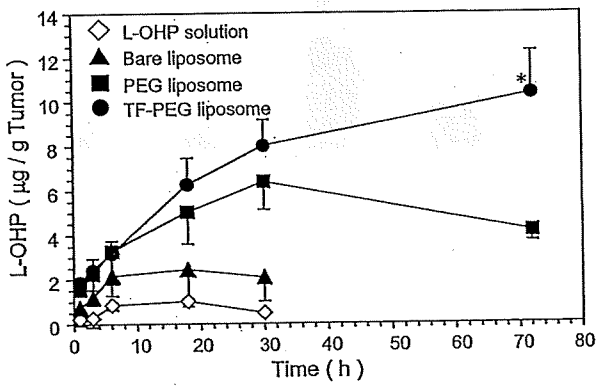

Fig. 4. Time course of tumor accumulation of L-OHP in Colon 26-bearing mice. L-OHP in solution or encapsulated within Bare-, PEG- or TF–PEG-liposomes (L-OHP: 5 mg/kg weight) was injected via tail veins of Colon 26-bearing mice. At various times thereafter, tumor tissue was collected from the mice. Concentrations of L-OHP in the tumor tissues were measured by MIP-MS. Data are shown as means and standard deviation ($n=3$). *$P<0.05$ (PEG-liposomes vs. TF–PEG-liposomes).

Fig. 4 shows the time course of L-OHP in Colon 26 solid tumor tissue after i.v. injection of L-OHP in solution and encapsulated within Bare-, PEG- or TF–PEG-liposomes. The concentrations of L-OHP in tumor tissue at 18 h after i.v. injection of L-OHP in solution and in Bare-liposomes were 0.98 and 2.1 μg/g tumor, respectively, and did not increase thereafter. The concentrations of L-OHP encapsulated within PEG- and TF–PEG-liposome in tumor tissue were even higher than that of L-OHP in solution and in Bare-liposomes. The L-OHP concentration in tumor tissue decreased 30 h after i.v. injection of L-OHP encapsulated within PEG-liposomes. Interestingly, the profiles of L-OHP encapsulated within TF–PEG- and PEG-liposomes in tumor tissues differed. The concentration of L-OHP encapsulated within TF–PEG-liposomes continued to increase until 72 h after i.v. injection and a high L-OHP concentration was maintained in the tumor for a longer period.

3.3. Assessment of side effects for L-OHP encapsulated within TF–PEG-liposomes

The circulation of L-OHP in the blood was prolonged when encapsulated within PEG- and TF–PEG-liposomes and the biodistribution of L-OHP encapsulated within liposomes differed from that of free L-OHP. We confirmed that liposomal L-OHP was distributed to major tissues. Thus unexpected side effects might arise when liposomal L-OHP is injected. To determine the toxicity of liposomal L-OHPs *in vivo*, we measured levels of serum albumin, total protein, GOT, GPT and BUN (Table 1). GOT, GPT and BUN are the markers of toxicity for liver. In addition, GOT is utilized as the marker of toxicity for heart. Moreover, BUN is mainly the marker of kidney. The BUN levels of mice injected with liposomal L-OHP did not differ from those of control mice injected with saline. We therefore considered that liposomal L-OHPs did not cause significant toxicity for liver and kidney. Furthermore, the other biochemical parameters tested in mice injected with liposomal L-OHPs did not significantly differ as compared with non-treated and saline-injected mice.

3.4. Therapeutic effect of L-OHP encapsulated within TF–PEG-liposomes

Mice bearing Colon 26 tumors were injected with L-OHP in solution or encapsulated within various liposomes and the therapeutic effects were examined by measuring the suppression of tumor growth (Fig. 5). Tumor growth was somewhat suppressed to a similar extent by L-OHP in solution and encapsulated within Bare- or PEG-liposomes, but obviously suppressed by L-OHP encapsulated within TF–PEG-liposomes.

4. Discussion

L-OHP is a cisplatin derivative that was designed to improve side effects such as toxicity to the kidney and peripheral nerve system. However, most L-OHP in the whole blood of mice injected with L-OHP in solution was taken up by erythrocytes, so that the levels of free L-OHP in plasma were very

Table 1
Serum biochemistry of mice injected with L-OHP in solution and encapsulated within Bare-, PEG- or TF–PEG-liposomes

	Time after injection (days)	Albumin (g/dL)	Total protein (g/dL)	GOT (IU/L)	GPT (IU/L)	BUN (mg/dL)
Normal		3.1 (0.1)	4.3 (0.3)	51.3 (6.4)	29.6 (3.9)	15.9 (2.3)
Saline	3	2.8 (0.3)	4.3 (0.3)	43.0 (4.2)	29.0 (7.5)	22.9 (0.2)
Solution	3	2.8 (0.2)	4.4 (0.1)	45.5 (7.7)	27.2 (1.4)	16.7 (4.7)
Bare	3	2.8 (0.1)	4.4 (0.1)	44.8 (11.7)	22.8 (3.1)	20.8 (2.8)
PEG	3	2.9 (0.1)	4.4 (0.0)	41.6 (4.4)	27.3 (3.3)	18.3 (1.1)
TF–PEG	3	2.8 (0.1)	4.5 (0.2)	41.2 (3.3)	23.3 (3.4)	19.3 (0.7)

L-OHP (5 mg/kg) was injected via tail veins of Colon 26-bearing mice. Blood samples were collected from veins of fundus oculi on 3 days after injection of L-OHP, and serum samples were isolated from blood samples by centrifugation. Serum albumin, total protein, GOT, GPT and BUN were measured using respective kits. Data are shown as means and standard deviation ($n=3$).

low. Pendyala and Creaven revealed that erythrocytes do not serve as reservoirs of partitioned drugs (Pendyala and Creaven, 1993). Thus, to maintain a therapeutic concentration of free L-OHP *in vivo* after injecting L-OHP in solution is difficult. Thus, L-OHP should be delivered directly to tumor cells to exert a powerful anti-tumor effect. The TF–PEG-liposomes encapsulating L-OHP that we prepared here appear to satisfy these requirements and should be very useful for cancer chemotherapy. We found that injected TF–PEG-liposomes resulted in a high concentration of L-OHP being maintained in mouse tumor tissue, and that tumor growth was more suppressed than with PEG-liposomes, Bare-liposomes and free L-OHP in solution. We previously reported that TF–PEG-liposomes are useful as a carrier targeting the cytoplasm of tumor cells *in vitro* and *in vivo* (Ishida et al., 1999, 2001; Iinuma et al., 2002; Hatakeyama et al., 2004; Kakudo et al., 2004; Maruyama et al., 2004; Miyajima et al., 2006). Tumor growth potential is reflected by abundant TF receptors in cancerous cells (Huebers and Finch, 1987). Thus, TF receptors might be a viable target molecule for therapy. We found between 2.5 and 5×10^5 surface TF receptors per Colon 26 cell (data not shown) (Ishida et al., 2001). Indeed, L-OHP encapsulated within TF–PEG-liposomes suppressed tumor cell growth *in vitro* and the suppression was abrogated by adding an excess of free TF into the medium. TF–PEG-liposome had about TF 20–25 molecules per liposome (Ishida et al., 2001). In this study, we showed that TF–PEG-liposomes were effectively internalized via TF receptor-mediated endocytosis, so that a large amount of L-OHP was introduced into cytoplasm of tumor cells.

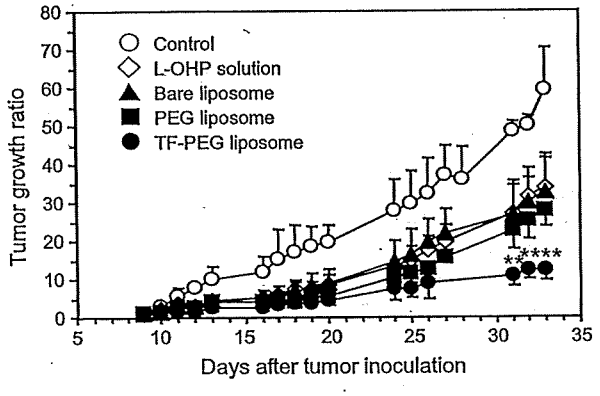

Fig. 5. Comparison of tumor growth suppression with L-OHP in solution and in liposomes in Colon 26-bearing mice. L-OHP solution or L-OHP encapsulated within Bare-, PEG- or TF–PEG-liposomes (L-OHP: 5 mg/kg) was injected via tail veins of Colon 26-bearing mice on days 9 and 12 after tumor cell inoculation. Tumor growth ratio was calculated as described in Section 2. Data are shown as means and standard deviation ($n=4$). $^{**}P<0.01$ (PEG-liposomes vs. TF–PEG-liposomes).

Intravenous injection of liposomal L-OHP into tumor-bearing mice resulted in increased L-OHP accumulation in solid tumors compared with free L-OHP. This phenomenon is referred to as the EPR effect of long circulating liposomes in solid tumor tissues. The most likely mechanism is the increased amount of time that the liposomes circulate in the blood and the leaky nature of the microvasculature in solid tumor tissues. We previously found that the size of the liposomes is an important factor for extravasation (Ishida et al., 1999). The circulation of TF–PEG- and PEG-liposomes with an average diameter of 100–200 nm was the most prolonged and the tumor accumulation was the highest. Thus, the accumulation of TF–PEG- and PEG-liposomes in tumor tissues is directly associated with the AUC_{blood} of the plasma clearance (Ishida et al., 2001; Maruyama et al., 2004). In this regard, a low AUC_{blood} due to high uptake of Bare-liposomes by the RES would lead to low tumor accumulation (Maruyama et al., 2004), even if the tumor vasculature were leakier than normal tissue. In other words, only small liposomes (about 100–200 nm mean diameter) with prolonged blood circulation would reach extravascular target sites (Ishida et al., 1999). Effective anti-tumor therapy by L-OHP requires its internalization into the cytoplasm of tumor cells because this drug works via the inhibition of DNA synthesis and transcription by forming DNA adducts (Pendyala et al., 1995). The therapeutic effects of PEG-liposomes and of L-OHP in solution were similar. We therefore considered that PEG-liposomes could deliver L-OHP to tumor tissue through the EPR effect, but were not effectively internalized into the cytoplasm. In contrast, TF–PEG-liposomes appeared to deliver L-OHP into the cytoplasm of tumor cells via TF receptor-mediated endocytosis after extravasation by the EPR effect (Ishida et al., 2001). Actually, the amount of time that PEG- and TF–PEG-liposomes remained in tumor tissues differed despite prolonged long circulation in the blood. These results supported the notion that TF–PEG-liposomes deliver L-OHP to the surface and the interior of tumor cells. Prolonged circulation of TF–PEG-liposomes in the blood increased the amount of time that L-OHP was exposed to various tissues including tumors. In addition, it was reported that TF receptors were also expressed normal cells such as the

hepatocyte and endothelial cells in the brain (Jefferies et al., 1984; Bomford and Munro, 1985). We considered the possibility of a concomitant increase in the incidence of acute toxicity after L-OHP single i.v. injection in Table 1. However, blood biochemistry tests revealed that the tested parameters remained within the normal range. These findings indicated that L-OHP encapsulated within TF–PEG-liposomes did not induce any significant acute toxicity in the presence of increased distribution to the liver compared with L-OHP in solution. We also examined about the biodistribution of L-OHP encapsulated within TF–PEG-liposomes in other experiment, the concentration of L-OHP in the brain was very low (about 0.06 μg/g tissue) at 72 h after i.v. injection of the liposomes. Actually, abnormal behaviors were not observed in the mice. Therefore, it was thought that significant side effects were not induced in the brain. In addition, we did not observe the remarkable decreasing of body weight after i.v. injection two times of L-OHP using the liposomes in Fig. 5. These results indicated that the frequency of serious side effects was minimal.

Although L-OHP is a useful anti-tumor drug, it is rapidly cleared from the blood. We addressed this issue by using TF–PEG-liposomes as a carrier of L-OHP. In addition, electron microscopic studies in Colon 26 tumor-bearing mice revealed that the extravasated TF–PEG-liposomes were internalized into tumor cells by receptor-mediated endocytosis (Ishida et al., 2001). Considering these results of electron microscopic studies, it was thought that TF–PEG-liposomes effectively delivered L-OHP into the cytoplasm of tumor cells bearing TF receptors. To our knowledge, we are the first to show a therapeutic effect of L-OHP against solid tumors using TF–PEG-liposomes as the carrier.

Kono et al. developed a polymer with fusogenic ability at low pH (Kono et al., 1997). In addition, another group reported that dioleoyl phosphatidylethanolamine (DOPE) can also destabilize endosomal membranes depending on endosomal pH. Thus, if the polymer and/or DOPE are applied to TF–PEG-liposomes with encapsulated L-OHP, the efficiency of L-OHP delivery into cytoplasm might increase. Further optimization of TF–PEG-liposomes encapsulating L-OHP should eventually result in the development of a highly effective cancer therapy.

In conclusion, TF–PEG-liposomes, which allow both passive and active targeting, might be a potential carrier for *in vivo* cytoplasmic targeting of L-OHP in mice with solid tumors overexpressing surface TF receptors. We believe that TF–PEG-liposomes show promise in the clinical environment as an ideal carrier for chemotherapy against various types of tumors that overexpress TF receptors.

Acknowledgments

We thank Dr. Y. Kidani for the gift of the L-OHP. Part of this study was supported by a Grant-in-Aid for Cancer Research (No. 12-1 to Kazuo Maruyama) from the Ministry of Health, Labor and Welfare, Japan, and the investigation was performed as trust study of the National Institute of Biomedical Innovation.

References

Aisen, P., 1994. The transferrin receptor and the release of iron from transferrin. Adv. Exp. Med. Biol. 356, 31–40.

Bomford, A.B., Munro, H.N., 1985. Transferrin and its receptor: their roles in cell function. Hepatology 5, 870–875.

Durant, J.R., 1980. Cisplatin: a clinical overview. In: Prestayko, A.W., Crooke, S.T., Cater, S.K. (Eds.), Cisplatin: Current Status and New Developments, pp. 317–321.

Dvorak, H.F., Nagy, J.A., Dvorak, J.T., Dvorak, A.M., 1988. Identification and characterization of the blood vessels of solid tumors that are leaky to circulating macromolecules. Am. J. Pathol. 133, 95–109.

Extra, J.M., Espie, M., Calvo, F., Ferme, C., Mignot, L., Marty, M., 1990. Phase I study of oxaliplatin in patients with advanced cancer. Cancer Chemother. Pharmacol. 25, 299–303.

Goldberg, R.M., Sargent, D.J., Morton, R.F., Fuchs, C.S., Ramanathan, R.K., Williamson, S.K., Findlay, B.P., Pitot, H.C., Alberts, S.R., 2004. A randomized controlled trial of fluorouracil plus leucovorin, irinotecan, and oxaliplatin combinations in patients with previously untreated metastatic colorectal cancer. J. Clin. Oncol. 22, 23–30.

Hatakeyama, H., Akita, H., Maruyama, K., Suhara, T., Harashima, H., 2004. Factors governing the in vivo tissue uptake of transferrin-coupled polyethylene glycol liposomes in vivo. Int. J. Pharm. 281, 25–33.

Huebers, H.A., Finch, C.A., 1987. The physiology of transferrin and transferrin receptors. Physiol. Rev. 67, 520–582.

Iinuma, H., Maruyama, K., Okinaga, K., Sasaki, K., Sekine, T., Ishida, O., Ogiwara, N., Johkura, K., Yonemura, Y., 2002. Intracellular targeting therapy of cisplatin-encapsulated transferring–polyethylene glycol liposome on peritoneal dissemination of gastric cancer. Int. J. Cancer 99, 130–137.

Ishida, O., Maruyama, K., Sasaki, K., Iwatsuru, M., 1999. Size-dependent extravasation and interstitial localization of polyethyleneglycol liposomes in solid tumor-bearing mice. Int. J. Pharm. 190, 49–56.

Ishida, O., Maruyama, K., Tanahashi, H., Iwatsuru, M., Sasaki, K., Eriguchi, M., Yanagie, H., 2001. Liposomes bearing polyethyleneglycol-coupled transferrin with intracellular targeting property to the solid tumors in vivo. Pharm. Res. 18, 1042–1048.

Jain, R.K., Gerlowski, L.E., 1986. Extravascular transport in normal and tumor tissues. Crit. Rev. Oncol. Hematol. 5, 115–170.

Jefferies, W.A., Brandon, M.R., Hunt, S.V., Williams, A.F., Gatter, K.C., Mason, D.Y., 1984. Transferrin receptor on endothelium of brain capillaries. Nature 312, 162–163.

Kakudo, T., Chaki, S., Futaki, S., Nakase, I., Akaji, K., Kawakami, T., Maruyama, K., Kamiya, H., Harashima, H., 2004. Transferrin-modified liposomes equipped with a pH-sensitive fusogenic peptide: an artificial viral-like delivery system. Biochemistry 43, 5618–5628.

Kidani, Y., Noji, M., Tashiro, T., 1980. Antitumor activity of platinum(II) complexes of 1,2-diamino-cyclohexane isomers. Gann 71, 637–643.

Kono, K., Igawa, T., Takagishi, T., 1997. Cytoplasmic delivery of calcein mediated by liposomes modified with a pH-sensitive poly(ethylene glycol) derivative. Biochim. Biophys. Acta 1325, 143–154.

Machover, D., Diaz-Rubio, E., de Gramont, A., Schilf, A., Gastiaburu, J.J., Brienza, S., Itzhaki, M., Metzger, G., N'Daw, D., Vignoud, J., Abad, A., Francois, E., Gamelin, E., Marty, M., Sastre, J., Seitz, J.F., Ychou, M., 1996. Two consecutive phase II studies of oxaliplatin (L-OHP) for treatment of patients with advanced colorectal carcinoma who were resistant to previous treatment with fluoropyrimidines. Ann. Oncol. 7, 95–98.

Maruyama, K., Ishida, O., Kasaoka, S., Takizawa, T., Utoguchi, N., Shinohara, A., Chiba, M., Kobayashi, H., Eriguchi, M., Yanagie, H., 2004. Intracellular targeting of sodium mercaptoundecahydrododecaborate (BSH) to solid tumors by transferrin–PEG liposomes, for boron neutron-capture therapy (BNCT). J. Control. Rel. 98, 195–207.

Maruyama, K., Takahashi, N., Tagawa, T., Nagaike, K., Iwatsuru, M., 1997. Immunoliposomes bearing polyethyleneglycol-coupled Fab' fragment show prolonged circulation time and high extravasation into targeted solid tumors in vivo. FEBS Lett. 413, 177–180.

Maruyama, K., Takizawa, T., Yuda, T., Kennel, S.J., Huang, L., Iwatsuru, M., 1995. Targetability of novel immunoliposomes modified with amphipathic

poly(ethylene glycol)s conjugated at their distal terminals to monoclonal antibodies. Biochim. Biophys. Acta 1234, 74–80.

Maruyama, K., Unezaki, S., Takahashi, N., Iwatsuru, M., 1993. Enhanced delivery of doxorubicin to tumor by long-circulating thermosensitive liposomes and local hyperthermia. Biochim. Biophys. Acta 1149, 209–216.

Mathe, G., Kidani, Y., Segiguchi, M., Eriguchi, M., Fredj, G., Peytavin, G., Misset, J.L., Brienza, S., de Vassals, F., Chenu, E., et al., 1989. Oxalatoplatinum or 1-OHP, a third-generation platinum complex: an experimental and clinical appraisal and preliminary comparison with *cis*-platinum and carboplatinum. Biomed. Pharmacother. 43, 237–250.

Matsumura, Y., Maeda, H., 1986. A new concept for macromolecular therapeutics in cancer chemotherapy: mechanism of tumoritropic accumulation of proteins and the antitumor agent smancs. Cancer Res. 46, 6387–6392.

Miyajima, Y., Nakamura, H., Kuwata, Y., Lee, J.D., Masunaga, S., Ono, K., Maruyama, K., 2006. Transferrin-loaded nido-carborane liposomes: tumor-targeting boron delivery system for neutron capture therapy. Bioconjug. Chem. 17, 1314–1320.

Pendyala, L., Creaven, P.J., 1993. In vitro cytotoxicity, protein binding, red blood cell partitioning, and biotransformation of oxaliplatin. Cancer Res. 53, 5970–5976.

Pendyala, L., Kidani, Y., Perez, R., Wilkes, J., Bernacki, R.J., Creaven, P.J., 1995. Cytotoxicity, cellular accumulation and DNA binding of oxaliplatin isomers. Cancer Lett. 97, 177–184.

Rothenberg, M.L., Oza, A.M., Bigelow, R.H., Berlin, J.D., Marshall, J.L., Ramanathan, R.K., Hart, L.L., Gupta, S., Garay, C.A., Burger, B.G., Le Bail, N., Haller, D.G., 2003. Superiority of oxaliplatin and fluorouracil–leucovorin compared with either therapy alone in patients with progressive colorectal cancer after irinotecan and fluorouracil–leucovorin: interim results of a phase III trial. J. Clin. Oncol. 21, 2059–2069.

Tashiro, T., Kawada, Y., Sakurai, Y., Kidani, Y., 1989. Antitumor activity of a new platinum complex, oxalato(*trans*-L-1,2-diaminocyclohexane)platinum(II): new experimental data. Biomed. Pharmacother. 43, 251–260.

Wagner, E., Curiel, D., Cotton, M., 1994. Delivery of drugs, proteins and genes into cells using transferrin as a ligand for receptor-mediated endocytosis. Adv. Drug Deliv. Rev. 14, 113–135.

Autophagy Is Activated in Colorectal Cancer Cells and Contributes to the Tolerance to Nutrient Deprivation

Kazunori Sato,[1,3] Katsuya Tsuchihara,[1] Satoshi Fujii,[2] Masanori Sugiyama,[3] Tomoyuki Goya,[3] Yutaka Atomi,[3] Takashi Ueno,[4] Atsushi Ochiai,[2] and Hiroyasu Esumi[1]

[1]Cancer Physiology Project and [2]Pathology Division, Research Center for Innovative Oncology, National Cancer Center Hospital East, Chiba, Japan and [3]Department of Surgery, Kyorin University School of Medicine; [4]Department of Biochemistry, Juntendo University School of Medicine, Tokyo, Japan

Abstract

Several types of cancer cells, including colorectal cancer–derived cell lines, show austerity, the resistance to nutrient starvation, but exactly how cancer cells obtain energy sources under conditions in which their external nutrient supply is extremely limited remains to be clarified. Because autophagy is a catabolic process by which cells supply amino acids from self-digested organelles, cancer cells are likely to use autophagy to obtain amino acids as alternative energy sources. Amino acid deprivation-induced autophagy was assessed in DLD-1 and other colorectal cancer–derived cell lines. The autophagosome-incorporated LC3-II protein level increased after treatment with a combination of autolysosome inhibitors, which interferes with the consumption of autophagosomes. Autophagosome formation was also morphologically confirmed using ectopically expressed green fluorescent protein-LC3 fusion proteins in DLD-1 and SW480 cells. These data suggest that autophagosomes were actively produced and promptly consumed in colorectal cancer cells under nutrient starvation. Autolysosome inhibitors and 3-methyl adenine, which suppresses autophagosome formation, remarkably enhanced apoptosis under amino acid–deprived and glucose-deprived condition. Similar results were obtained in the cells with decreased ATG7 level by the RNA interference. These data suggest that autophagy is pivotal for the survival of colorectal cancer cells that have acquired austerity. Furthermore, autophagosome formation was seen only in the tumor cells but not in the adjacent noncancerous epithelial cells of colorectal cancer specimens. Taken together, autophagy is activated in colorectal cancers *in vitro* and *in vivo*, and autophagy may contribute to the survival of the cancer cells in their microenvironment. [Cancer Res 2007;67(20):9677–84]

Introduction

Proliferating cancer cells require nutrients for growth. Tumor angiogenesis is one way to increase the blood flow to supply the required oxygen and energy source to the growing tumor tissues. However, recent studies have revealed that oxygen and glucose levels are frequently reduced in locally advanced tumors even after tumor vessels have been established (1–3). It suggests that the tumor microvasculature is structurally and functionally abnormal and not sufficient to supply the blood flow needed by proliferating cancer cells. Furthermore, some aggressive malignant tumors, such as pancreatic cancers, are clinically hypovascular (4). Under these conditions, cancer cells are likely to encounter a shortage of nutrients. These cells might use some alternative metabolic process to obtain energy for their survival. We have reported that several cancer cell lines, including pancreatic cancer–derived and colorectal cancer–derived cell lines, are resistant to the nutrient-deprived culture condition. For example, colon cancer–derived SW480 and DLD-1 cells showed >50% survival after 36 h of culture in a glucose-deprived, amino acid–deprived, and serum-deprived medium. On the other hand, untransformed human fibroblasts and liver cancer–derived cells were completely abolished under the same condition. We named this starvation-resistant phenotype "austerity" and speculated that this phenomenon may contribute to the survival of cancer cells in nutrient-deficient microenvironment (5, 6).

It remains to be elucidated how cancer cells obtain energy sources under the condition in which the supply of external nutrients is extremely limited. Mammalian cells are able to use amino acids as an alternative energy source. If the starvation-resistant cancer cells can raise amino acids from the inside of cells, the amino acids become potential energy sources under such condition.

Autophagy is a conserved catabolic process by which cells self-digest their organelles (7). At the first step of autophagy, a lipid bilayer structure called the isolation membrane is developed. Isolation membrane sequesters cytoplasmic materials, such as organelles, to form autophagosomes. During this step, LC3, one of the mammalian homologues of yeast ATG8, is processed and activated by an ubiquitination-like reaction regulated by ATG7 and ATG3 (8). First, LC3 proform is cleaved into a soluble form known as LC3-I. LC3-I is further modified into a membrane-bound form, LC3-II, and recruited onto the autophagosomes. Autophagosomes engulfing organelles then fuse with lysosomes and mature into autolysosomes. Sequestrated materials are digested to amino acids in the autolysosomes by the lysosomal enzymes. In this step, LC3 and other autophagosome components are also digested and diminished. Several pharmacologic autophagy inhibitors have been used to evaluate the physiologic relevance of autophagy in culture cells. The combination of E64d and pepstatin A inhibits lysosomal enzymes and interferes with autolysosomal digestion, whereas 3-methyladenine (3-MA) blocks autophagosome formation to inhibit autophagy (9).

Autophagy has roles in protecting cells against shortage of nutrients. Cells supply amino acids from self-digested organelles as an alternative energy source for their survival (7). This function of autophagy seems ideal to foster cancer cells to survive in an unfavorable starved microenvironment. However, the physiologic

Note: Supplementary data for this article are available at Cancer Research Online (http://cancerres.aacrjournals.org/).

Requests for reprints: Hiroyasu Esumi, National Cancer Center Hospital East, 6-5-1 Kashiwanoha, Kashiwa, Chiba 277-8577, Japan. Phone: 81-4-7134-6901; Fax: 81-4-7134-8676; E-mail: hesumi@east.ncc.go.jp.

doi:10.1158/0008-5472.CAN-07-1462

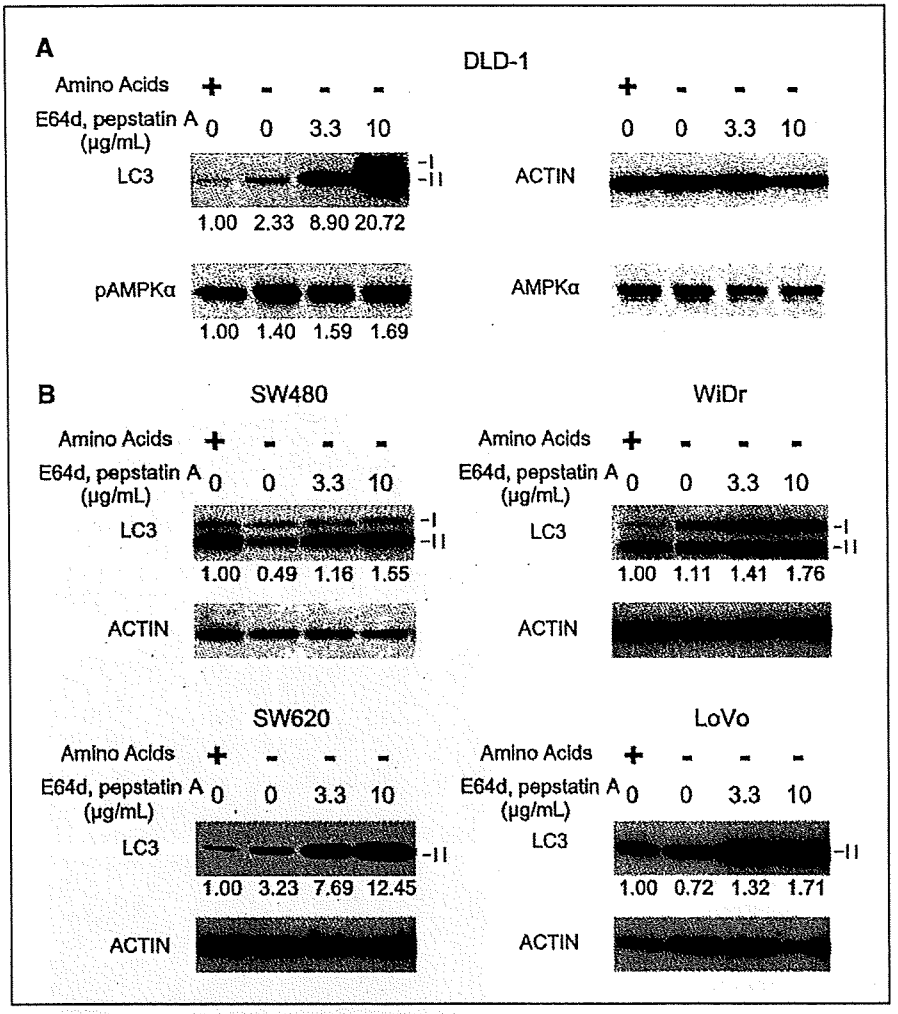

Figure 1. Amino acid starvation induced accumulation of autophagosome-incorporated LC3-II in cultured colorectal cancer–derived cell lines. *A*, DLD-1 cells were cultured in amino acid–containing or amino acid–deprived medium. Lysosomal protease inhibitors E64d and pepstatin A were added at the indicated concentration. Total cell lysates were collected at 24 h after incubation and submitted for Western blotting to detect phosphorylated AMPKα and LC3 proteins. *I*, LC3-I; *II*, LC3-II. Phosphorylated AMPKα density was standardized by total AMPKα, and LC3-II density was standardized by actin. *B*, colorectal cancer–derived cell lines WiDr, SW620, SW480, and LoVo were treated as above. LC3 proteins were detected and measured by Western blotting.

relevance of autophagy in tumor formation and progression is still controversial. We hypothesized that autophagy contributes to the acquisition of austerity in cancer cells and investigated whether autophagic machinery is activated in colorectal cancer cells and tissues. We also examined whether the inhibition of autophagy induced death of colorectal cancer cells, which had acquired austerity.

Materials and Methods

Cells and culture. Human colorectal cancer cell lines SW480, DLD-1, WiDr, SW620, and LoVo were purchased from the American Type Culture Collection. Cells were maintained in DMEM (Invitrogen) supplemented with 10% FCS, 4.5 g/L glucose, and antibiotics. Amino acid starvation was done with an amino acid–deprived medium as described previously (6). E64d, pepstatin A, and 3-methyl adenine (3-MA) were purchased from Sigma.

Patients and tissue samples. Subjects comprised 65 patients with 80 adenocarcinomas, who underwent surgical removal of colorectal cancer in the National Cancer Center Hospital East (Kashiwa, Japan) from 2004 to 2006. Twenty tubular adenomas and 13 hyperplastic polyps, which were endoscopically resected, were also collected. All patients agreed to enrollment in the study and each gave informed consent. The institutional review board of the National Cancer Center approved all protocols on the patients' agreement. In the present study, only tumors that have penetrated through muscularis mucosae into submucosa are considered adenocarcinoma according to the WHO classification. Tubular adenomas were also classified into low grade or high grade, depending on the degree of glandular complexity, extent of nuclear stratification, and severity of abnormal nuclear morphology (WHO classification).

Western blotting. Production of rabbit polyclonal LC3 and ATG7 antibodies was described previously (8, 10). Phosphorylated Akt (Ser^{473}) and phosphorylated AMPKα1 (Ser^{485}) antibodies were purchased from Cell Signaling Technology. Cellular protein was extracted from culture cells and tissue specimens using lysis buffer [1% SDS, 10 mmol/L Tris-HCl (pH 7.4), 1 mmol/L Na_3VO_4], and protein concentration was determined with a bicinchoninic acid protein assay kit (Pierce). Ten micrograms of total cell lysates were separated by 15% Tris-glycine SDS-PAGE and then transferred to a polyvinylidene difluoride membrane. Membranes were blocked with TBS containing 5% (w/v) dry milk and 2% (w/v) bovine serum albumin with 0.1% Tween 20, washed with TBS containing 0.1% Tween 20 (TBST), and then incubated overnight at 4°C with 2 μg/mL of anti-LC3 antibody in 20 mmol/L Tris-HCl (pH 7.5), 0.15 mol/L NaCl, and 0.1% NaN_3. After washing in TBST, membranes were incubated for 1 h at room temperature with horseradish peroxidase–conjugated goat anti-rabbit IgG antibody (Santa Cruz Biotechnology) in 1:10,000. Signals were detected using enhanced chemiluminescence detection reagents (GE Healthcare). The density of each band was measured using ImageJ software (W.S. Rasband, ImageJ, NIH, Bethesda, MD).[5]

[5] http://rsb.info.nih.gov/ij/

Establishment of green fluorescent protein-LC3–expressing cells and detection of the fusion protein. A green fluorescent protein (GFP)-mouse LC3 fusion protein expressing vector pEGFP C2-LC3 was kindly provided by Dr. Hitoshi Okada (Ontario Cancer Institute, Toronto, Ontario, Canada). SW480 and DLD-1 cells (5×10^4 per well) were plated on six-well plates the day before transfection and 0.25 μg of plasmid DNA was transfected using TransFast Transfection Reagent (Promega) according to the manufacturer's protocol. Transfected cells were selected by 1 mg/mL of G418 sulfate (potency: 803 μg/mg; Calbiochem) for 14 days. GFP fusion proteins were observed using an LSM5 PASCAL laser scanning microscope system (Carl Zeiss Japan). Autophagosome-incorporated fusion proteins were measured using ImageJ software.

RNA interference. *ATG7* RNA interference was accomplished by transfecting DLD-1 cells with the specific small interfering RNA (siRNA). *ATG7*-targeting siRNA and nonsilencing siRNA were purchased from Dharmacon. Short oligo-RNAs were transfected using DharmaFECT 1 transfection reagent (Dharmacon) as recommended by the manufacturer. Cells were cultured for 48 h before analysis.

Cell death assay. Cell viability was assessed by the Hoechst 33342 (Sigma) staining as described previously (11). Treated cells were stained and examined under fluorescent microscopy. At least 1,000 cells were counted and distinguished as viable and apoptotic cells.

Immunohistochemistry. Tissue sections were deparaffinized and exposed to 3% hydrogen peroxide for 15 min to block endogenous peroxidase activity. For heat-induced epitope retrieval, the sections were placed in a 0.01 mol/L citrate buffer and heated at 120°C for 15 min. The nonspecific binding was blocked by preincubation with 2% normal swine serum in PBS (blocking buffer) for 60 min at room temperature. Individual slides were then incubated overnight at 4°C with an anti-LC3 antibody at a final concentration of 2 μg/mL in the blocking buffer. The slides were washed with PBS and then incubated with a peroxidase-labeled polymer conjugated to goat anti-rabbit IgG (DAKO EnVision Peroxidase Rabbit) for 45 min at room temperature. After extensive washing with PBS, the color reaction was developed in 2% 3,3′-diaminobenzidine in 50 mmol/L Tris buffer (pH 7.6) containing 0.3% hydrogen peroxide for 5 to 10 min. The sections were then counterstained with Meyer's hematoxylin, dehydrated, and mounted.

Transmission electron microscopy. Surgically resected tissue samples were fixed in ice-cold 2% glutaraldehyde and examined with a JEM-1011 transmission electron microscope (JEOL).

Statistical analysis. Data were analyzed using the Student's *t* test for statistical significance. *P* values were considered significant if <0.05. SD was calculated and represented in the bar graphs.

Results

Amino acid deprivation induced LC3-II accumulation in colorectal cancer cells. First, we assessed the induction of autophagy in colorectal cancer–derived culture cells. DLD-1 cells were cultured for 24 h in amino acid–deprived medium with or without a combination of lysosomal protease inhibitors E64d and pepstatin A. Amino acid deprivation induced increased phosphorylation of AMPKα in DLD-1 cells. Autolysosome inhibitors slightly enhanced the phosphorylation level of AMPKα (Fig. 1*A*). On the other hand, LC3-II level was slightly induced by amino acid deprivation, but addition of autolysosome inhibitors dramatically enhanced LC3-II level in a dose-dependent manner (Fig. 1*A*). Treatment with autolysosome inhibitors enhanced the accumulation of LC3-II in other colorectal cancer–derived cell lines, WiDr, SW620, and DLD-1 cells (Fig. 1*B*). The LC3-II level of SW480 and LoVo cells in amino acid–deprived medium without autolysosome inhibitors was less than that in amino acid–containing medium. However, the autolysosome inhibitors significantly increased LC3-II levels of these cells too (Fig. 1*B*).

Autophagosome formation was visualized using GFP-LC3 fusion protein. Then, we confirmed autophagosome formation in live cells. We established SW480 and DLD-1 cells that stably expressed the GFP-LC3 fusion protein. These cells were cultured in amino acid–deprived medium with or without the combination of E64d and pepstatin A for 12 h. The distribution of GFP-LC3 was determined by confocal fluorescent microscopy, and autophagosome-associated GFP-LC3 level was quantified (Fig. 2*A* and *B*). The GFP-LC3 fusion protein was observed as coarse dots in the cytoplasm of both SW480 and DLD-1 cells cultured in an amino acid–deprived medium. Consistent with the Western blotting data,

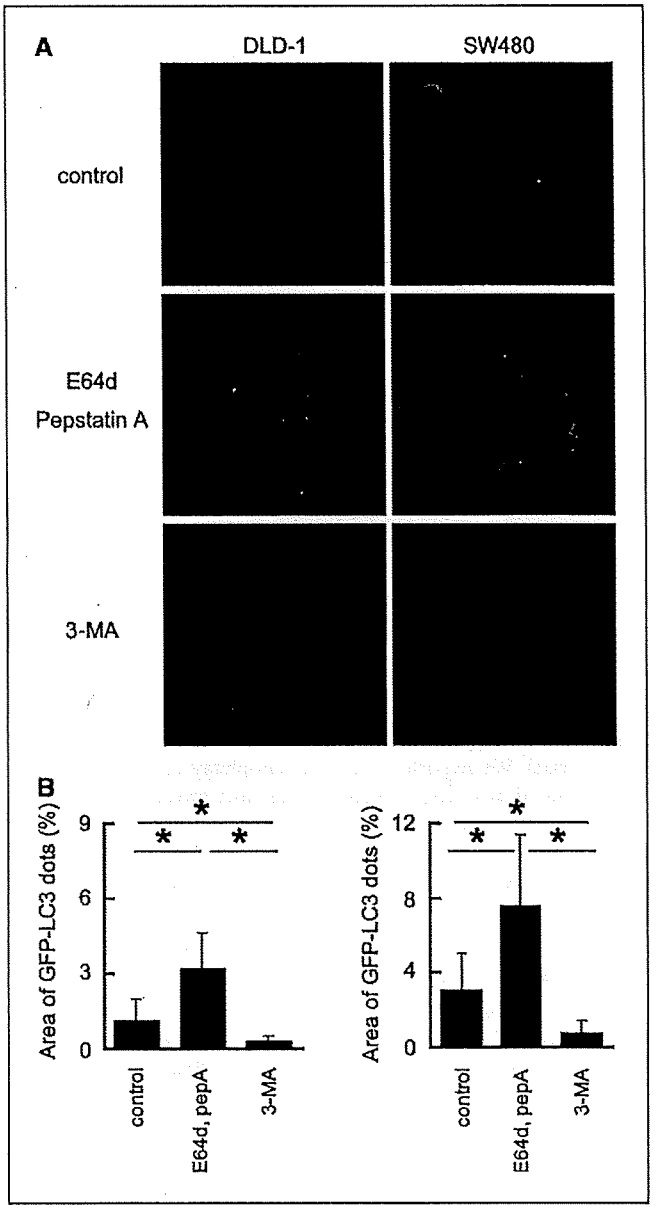

Figure 2. Autophagosome formation was visualized using GFP-LC3–expressing DLD-1 and SW480 cells. *A*, cells were incubated in amino acid–deprived medium with vehicle (DMSO), 10 μg/mL of E64d and pepstatin A, or 10 mmol/L of 3-MA for 12 h and observed under the confocal laser microscope. *B*, the area of coarse dots in the cytoplasm was measured and standardized in each cell. At least 100 cells were examined in each treatment. *pepA*, pepstatin A. *Columns*, mean percentage of dotted area; *bars*, SD. *, statistical significance ($P < 0.05$) in the Student's *t* test.

autolysosome inhibitor treatment enhanced the dot formation. In contrast, 3-MA, which inhibits autophagosome formation, significantly reduced the visible dots in the treated cells and redistributed GFP-LC3 to the cytoplasm. Taking these findings together, autophagosomes were properly produced, processed, and consumed in these colon cancer–derived cell lines under amino acid starvation.

Inhibition of autophagy induced apoptosis of colorectal cancer cell lines during nutrient starvation. To examine the effect of autophagy in tumor cell survival during nutrient starvation, the autophagy inhibitors were applied to examine the cell viability of SW480 and DLD-1 cells in amino acid–deprived medium. Hoechst 33342 staining showed limited death of both cell lines during 48-h culture in amino acid–deprived medium (Figs. 3 and 4*A*). On the contrary, addition of autolysosome inhibitors showed marked chromatin condensation, indicating apoptotic cell death (Fig. 3). This effect was dependent on the time of the treatment and dose of the inhibitors (Fig. 4*A*). Increased apoptosis was confirmed by flow cytometry with Annexin V and propidium iodide double staining (data not shown). 3-MA treatment also markedly induced chromatin condensation during amino acid starvation (Figs. 3 and 4*B*). Autolysosome inhibitors and 3-MA also induced apoptosis of SW620 cells in which functional autophagosome formation was confirmed (Figs. 1*B* and 4*B*). Similar results were obtained in the cells treated with *ATG7*-targeting siRNA. DLD-1 cells with decreased ATG7 expression showed increased apoptosis in amino acid–deprived medium (Fig. 4*C*). E64d and pepstatin A treatment enhanced apoptosis of DLD-1 in amino acid–deprived and glucose-deprived medium. However, these inhibitors did not affect the cell viability in nutrient-containing medium (Fig. 4*D*). These results strongly suggest that the autophagy has a protective role against nutrient deprivation-induced death of austeric colorectal cancer cells.

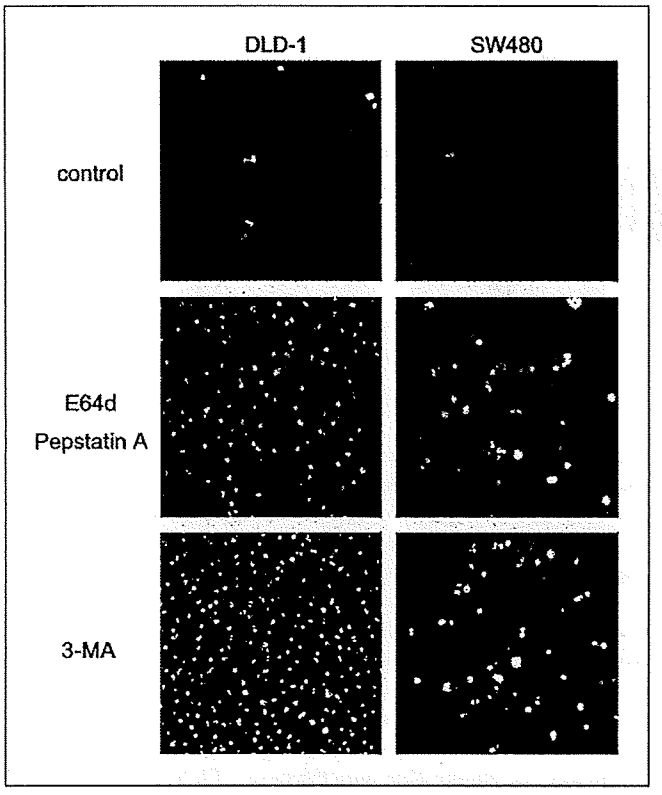

Figure 3. Autophagy inhibitors induced apoptosis of colorectal cancer cell lines during amino acid starvation. SW480 and DLD-1 cells were cultured in an amino acid–deprived medium with vehicle (DMSO), 10 μg/mL of E64d and pepstatin A, or 10 mmol/L of 3-MA for 48 h. Cells were stained with Hoechst 33342. Live cells show intact Hoechst 33342–positive (pale) nuclear staining pattern. Cells in apoptosis show chromatin condensation with dark Hoechst 33342–positive staining.

LC3-II is highly expressed in colorectal cancer tissues but not in normal epithelia. Because tumor cells are frequently exposed to nutrient starvation *in vivo*, we speculated that the protective role of autophagy may play some roles in tumor cell survival during tumorigenesis. We evaluated autophagy in surgically resected colorectal cancer tissues by detecting LC3. Paraffin-embedded samples of 65 cases with 80 adenocarcinoma lesions were examined by immunohistochemistry using an anti-LC3 antibody. Immunohistochemical expression for LC3 in tumor and normal epithelia was estimated by comparing the staining intensity in the submucosal or muscularis nerve plexus cells that consistently express LC3 (Fig. 5*A*). Tumor or nontumorous mucosal epithelia showing equal or stronger intensity than nerve cells were judged as "strongly positive," whereas the epithelia with weaker intensity than nerve cells were designated as "weakly positive." LC3 was not detected in the normal mucosa of all 65 patients. In contrast, we found positive staining for LC3 in the most of primary cancer tissues. In 80 adenocarcinomas, 59 were strongly positive and 13 were weakly positive. There was no significant difference of the LC3 positivity between well-differentiated and moderately differentiated adenocarcinomas (Fig. 5*A*; Table 1). Close examination of LC3-positive cells showed that the LC3 protein localized in the cytoplasm with irregular condensation (Fig. 5*A*). This distribution was similar to that of GFP-LC3 recruited onto autophagosomes in cultured colorectal cancer cells (Fig. 2). The LC3 status of metastatic lesions was also examined. Five metastatic adenocarcinomas of parietal lymph nodes were all LC3 positive (data not shown). Six metastatic adenocarcinomas in liver were also LC3 positive (Supplementary Figure). To confirm whether LC3 deposition reflects autophagosome formation, an LC3-positive adenocarcinoma specimen was examined with transmission electron microscopy. Cancer cells contained lipid bilayer structures engulfing organelles in the cytoplasm, which are characteristic for autophagosomes (Fig. 5*B*). To evaluate which type of LC3 was produced in cancer tissues, total cell lysates were prepared from five patients with surgically resected colorectal adenocarcinoma and LC3 was detected by Western blotting. A metastatic liver adenocarcinoma specimen and a noncancerous liver tissue specimen were also prepared from one patient. Autophagosome-incorporated LC3-II was a dominant form of LC3 in tumor tissues. Consistent with the immunohistochemical staining, the LC3-II level in four of five primary adenocarcinoma samples and in a metastatic adenocarcinoma sample in liver was higher than that in each corresponding noncancerous tissue, including liver (Fig. 5*C*). These results suggest that the autophagic machinery is activated in colorectal cancer tissues.

LC3 accumulation in benign tumors. We next examined LC3 positivity in benign tumors. LC3 was not accumulated in 13 hyperplastic polyps as well as the nontumorous mucosal epithelium. Among 10 high-grade tubular adenomas, 4 were negative, 5 were weakly positive, and 1 was strongly positive for LC3, whereas 10 low-grade tubular adenomas were negative for LC3 as well as nontumorous mucosal epithelium and hyperplastic polyps (Fig. 5*D*; Table 1).

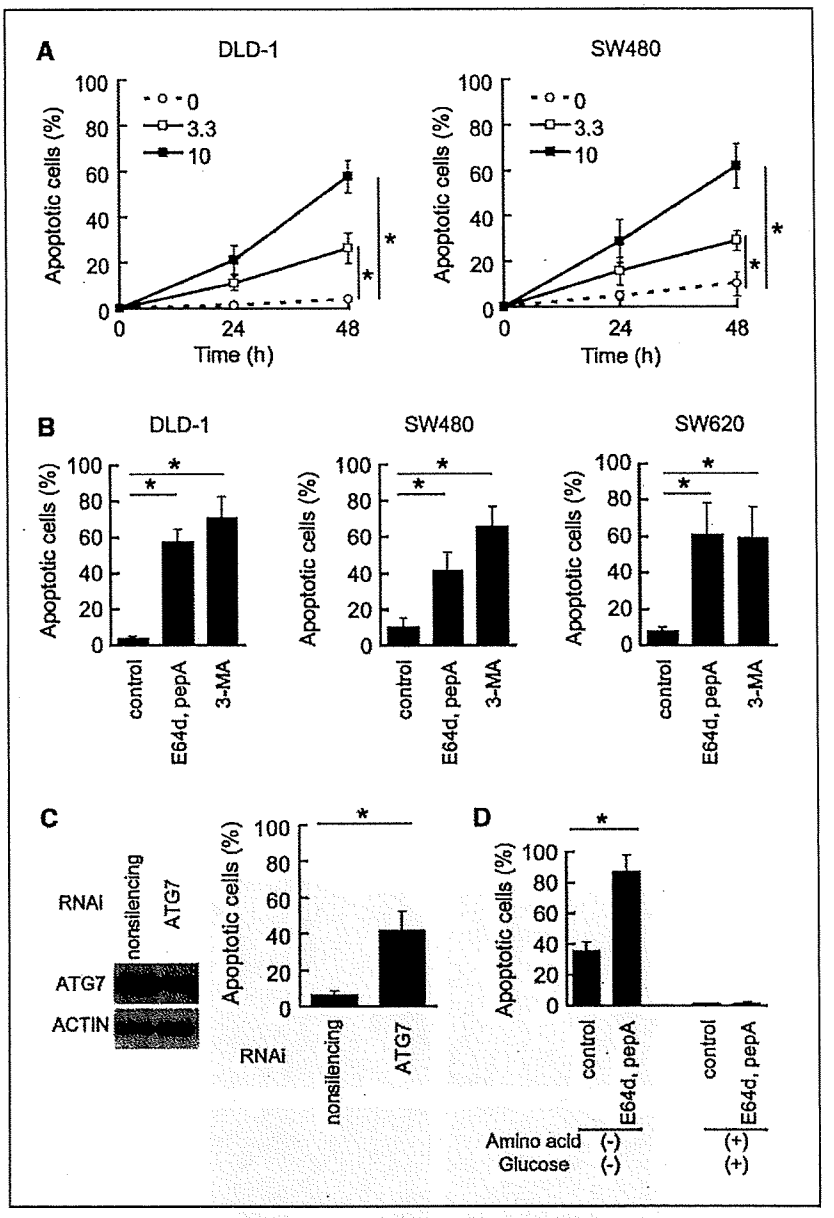

Figure 4. Inhibition of autophagy induced apoptosis. *A*, DLD-1 and SW480 cells were cultured in amino acid–deprived medium with vehicle (○) and 3.3 μg/mL (□) and 10 μg/mL (■) of E64d and pepstatin A. Cells were stained with Hoechst 33342 and the number of the apoptotic cells was counted. At least 1,000 cells were examined. *Points*, mean percentage of apoptotic cells ($n = 5$); *bars*, SD. *, statistical significance ($P < 0.05$) in the Student's *t* test. *B*, DLD-1, SW480, and SW620 cells were cultured in amino acid–deprived medium with 10 μg/mL of E64d and pepstatin A or 10 mmol/L of 3-MA for 48 h. Cells were stained with Hoechst 33342 and the number of the apoptotic cells was counted. At least 1,000 cells were examined. *Columns*, mean percentage of apoptotic cells ($n = 3$); *bars*, SD. *, statistical significance ($P < 0.05$) in the Student's *t* test. *C*, DLD-1 cells were transfected with nonsilencing siRNA and *ATG7*-siRNA. *Left*, ATG7 protein was specifically reduced in *ATG7*-siRNA–transfected cells; *right*, transfected cells were cultured in amino acid–deprived medium for 48 h and stained with Hoechst 33342. *RNAi*, RNA interference. *Columns*, mean percentage of apoptotic cells ($n = 3$); *bars*, SD. *, statistical significance ($P < 0.05$) in the Student's *t* test. *D*, DLD-1 cells were cultured in amino acid–containing and glucose-containing medium or amino acid–deprived and glucose-deprived medium with 10 μg/mL of E64d and pepstatin A for 48 h. *Columns*, mean percentage of apoptotic cells ($n = 3$); *bars*, SD. *, statistical significance ($P < 0.05$) in the Student's *t* test.

Discussion

The role of autophagy in the cell fate decision remains controversial. Autophagy is claimed to play roles in degradation of old cellular components, recycling constituents and responding to various cellular stresses especially those of energy deficiency (7). Recently, autophagy has attracted much attention in the connection with programmed cell death, autophagic death. Autophagic death eliminates damaged and/or harmful cells, such as cancer cells treated with anticancer reagents or the cells infected with pathogenic microorganisms (12, 13). On the other hand, autophagy is also claimed to be an indispensable physiologic reaction to sustain cell viability under nutrient-starved conditions (7).

The controversy about the physiologic roles of autophagy is also argued for cancer development and biology. In an experimental pancreas cancer model, increased autophagy was observed in the step of the tumor formation (14). Starvation-induced protein degradation was not down-regulated among transformed and transformed-tumorigenic bronchial epithelial cells compared with their normal counterparts (15). A high potential of autophagic protein degradation was observed in an undifferentiated colon cancer cell line HT29 (16). On the contrary, the basal rate of degradation of long-lived proteins in hepatoma cells was less than that of their noncancerous counterparts under normal nutrient condition (17, 18). Recently, several tumor-related gene products have been identified as autophagy regulators. The hemiallelic loss of *BECN*, a mammalian homologue of yeast *Atg6*, led to tumor formation in mammary glands, ovaries, and prostates (19). *BECN* coding protein, Beclin1, was later focused on as stimulating autophagy and suppressing tumorigenesis (20). It is suggested that mammalian target of rapamycin, which is regarded as a mediator of oncogenic signals, is involved in the negative control of autophagy (21). The *TP53* tumor suppressor gene product transactivates *DRAM*, which encodes a lysosomal protein that induces autophagy and is involved in p53-mediated cell death (22). These

contradictory findings suggest that there is not a unique paradigm about autophagy in tumorigenesis.

We have proposed that austerity is an important determinant of the malignancy of cancer (5, 6). Cancer cells with austerity can survive under conditions in which the exogenous nutrient supply is extremely limited. Under these conditions, cancer cells require alternative energy sources, such as amino acids. Autophagy is likely to be a way to supply amino acids for these cells.

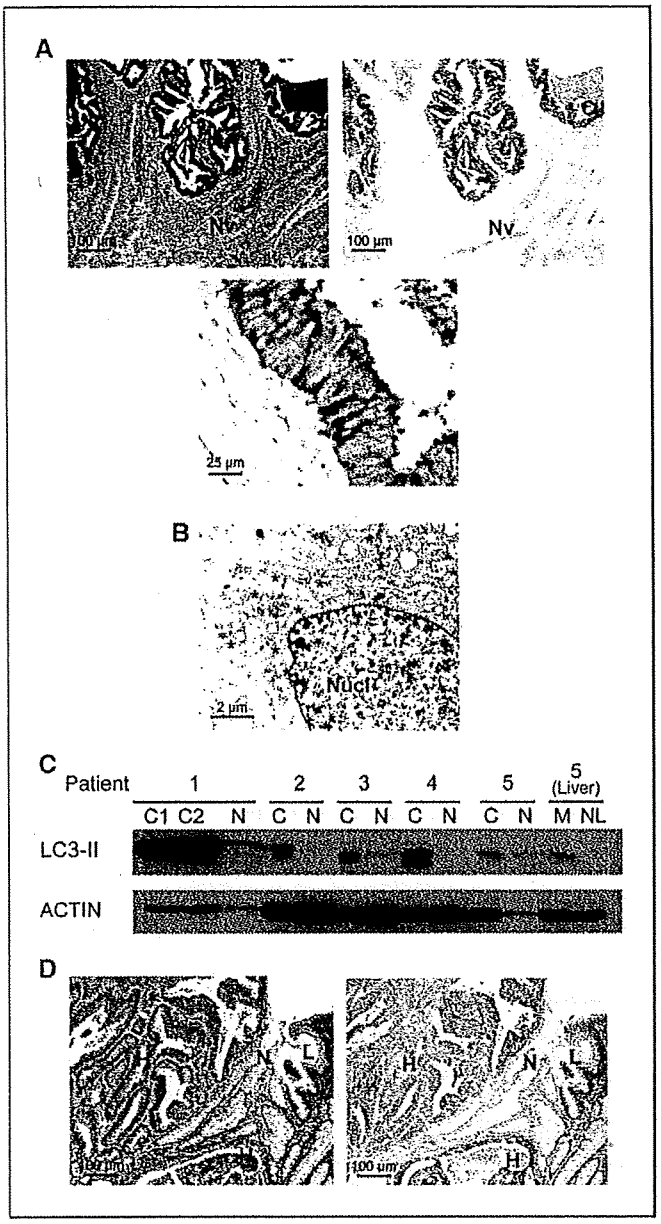

Figure 5. LC3-II was expressed in colorectal cancer tissues. *A*, LC3 protein was detected with immunohistochemistry using paraffin-embedded colon cancer samples. *Top left*, HE staining. Original magnification, ×100. *Top right*, LC3 immunostaining. Original magnification, ×100. LC3 was detected in cancer tissue (*C*) and intermuscular nerve cells (*Nv*). *Bottom*, magnified LC3-positive cancer tissue. Original magnification, ×400. *B*, ultrastructure of a surgically resected colon cancer shown by electron microscopy. Lipid bilayer structures engulfing organelles (*) are shown in the cytoplasm. *Nucl*, nucleus. Original magnification, ×2,000. *C*, total cell lysates were prepared from surgically resected primary and metastatic liver adenocarcinoma specimens and LC3-II was detected with Western blotting. *N*, noncancerous tissue; *M*, metastatic liver adenocarcinoma tissue; *NL*, noncancerous liver tissue. Case 1 had two independent primary tumors. *D*, LC3 was not detected in nonneoplastic tubules (*N*), whereas low-grade adenomatous component (*L*) showed weak LC3 positivity and high-grade adenomatous component (*H*) showed strong LC3 positivity. Original magnification, ×100.

In this study, we showed that colorectal cancer cells harbor functional autophagic machineries. The membrane-bound LC3-II protein level is regarded as a marker for the formation of autophagosomes (9, 23). We detected LC3-II with Western blotting using anti-LC3 antibody (Fig. 1). The autophagosome level is dynamically regulated in the cells undergoing autophagy. Under nutrient starvation, autophagosomes are rapidly degraded by lysosomal enzymes. The LC3-II level indicates the balance between the production and the consumption of autophagosomes. When the consumption is highly increased, the LC3-II level seems unchanged or even decreases comparing with that of non-autophagic cells. Interference of the degradation processes preserves LC3-II from consumption, and the accumulated LC3-II level reflects the amount of newly produced autophagosomes. In fact, amino acid deprivation without inhibitors slightly increased the LC3-II level in DLD-1 and SW620 cells, whereas there was no significant induction of LC3-II in WiDr, LoVo, and SW480 cells. However, treatment with autolysosome inhibitors markedly increased LC3-II in all tested cell lines. These data suggest that the autophagic machinery was functionally activated in a series of cultured colorectal cancer cells. Accumulation of autophagosomes was also visualized (Fig. 2). It has been reported that the GFP-fused LC3 protein was recruited to autophagosomes and degraded in autolysosomes as native LC3 proteins (23, 24). Recently, it was reported that transiently expressed fusion protein caused artificial accumulation in nonautophagic cells (25). To avoid the artifact, we prepared SW480 and DLD-1 cells stably expressing the GFP-LC3 protein. These cells showed characteristic dot formation in amino acid–deprived medium, suggesting that the fusion proteins were successfully recruited to the autophagosomes. Inhibition of autophagosome consumption by autolysosome inhibitors increased the dot formation of GFP-LC3 in SW480 and DLD-1 cells. In contrast, 3-MA, which interferes with autophagosome formation, apparently decreased the dots.

We showed that autophagy directly contributes to the survival of cancer cells under nutrient starvation. Both the autolysosome inhibitors and 3-MA induced marked apoptotic death of all examined colorectal cancer cells (Figs. 3 and 4). Interestingly, the concentration of inhibitors that induced cell death in nutrient-deprived medium did not affect the viability of the cells in the amino acid–containing medium. We observed that 3-MA successfully reduced the autophagosome formation in GFP-LC3–expressing SW480 cells in the amino acid–containing and glucose-containing medium (data not shown). This suggests that cancer cells may not depend on autophagy when sufficient nutrients are available, but suppression of autophagy is fatal in a starved environment. It was reported that inhibition of autolysosome function sensitized HeLa cells to apoptosis (26). Our observation was consistent with their findings. Furthermore, we suggest that autophagy has a pivotal role to acquiring the tolerance to amino acid deprivation in the cancer cells with austerity as well as the starvation-sensitive HeLa cells.

It has been well described that AMPK-mediated signaling pathway senses the intracellular energy status and regulates metabolism to maintain cellular homeostasis. We have reported that AMPK and its related kinases are key molecules to obtain austerity (27–29). Recently, it was reported that AMPK positively regulates autophagy (30). Activation of AMPK by amino acid

Table 1. LC3 expression in colorectal cancer tissues

	Total	Negative (%)	Weakly positive (%)	Strongly positive (%)
Adenocarcinoma				
Moderately	65	7 (10.8)	11 (16.9)	47 (72.3)
Well	15	1 (6.7)	2 (13.3)	12 (80.0)
Adenoma				
Low grade	10	10 (100)	0	0
High grade	10	4 (40)	5 (50)	1 (10)
Hyperplastic polyp	13	13 (100)	0	0
Nontumorous mucosa	65	65 (100)	0	0

deprivation was observed in DLD-1 cells in this study (Fig. 1*A*). We observed that glucose starvation also induces AMPKα phosphorylation in DLD-1 cells (data not shown), suggesting that depletion of amino acids and/or glucose induces decreased energy sources of cancer cells. Autolysosome inhibitors canceled the starvation-resistant phenotype in nutrient-deprived medium (Fig. 4). These findings strengthen the idea that autophagy provides intrinsic alternative energy sources and contributes to the survival of cancer cells under nutrient starvation.

Evaluating autophagy in clinical tumor samples has been difficult mainly due to the lack of appropriate autophagy-specific markers. In the present work, we showed that the LC3 immunohistochemical staining is a useful surrogate marker for autophagy in surgically resected cancer specimens. The LC3 protein was accumulated specifically in adenocarcinoma cells but not in surrounding nontumorous mucosal epithelial cells (Fig. 5). Accumulated LC3 protein was supposed to be involved in the autophagosome formation. Subcellular distribution of LC3 was similar to that of autophagosome-incorporated LC3 in culture cells. The majority of the LC3 protein was a membrane-bound LC3-II seen in Western blotting. In addition, the ultrastructure revealed the presence of autophagosomes in the cytoplasm.

Although LC3 accumulation showed a distinct contrast between adjacent nontumorous and tumor epithelial cells, the nutrient supply is assumed to be similar between these tissues. It suggests that the autophagy in colorectal cancer cells is regulated not only by the extracellular nutrients concentration but that some intrinsic mechanisms are also involved in the regulation. Aberrantly proliferating cancer cells require extra energy sources than normal cells. It is likely that the cells with active autophagy have an advantage for survival, especially when the cells do not have alternative ways to obtain extra energy sources, such as tumor angiogenesis.

If autophagy supplements energy sources in cancer cells, autophagosome formation might be increased as the nutrient starvation was extended. Degenhardt et al. reported an experimental cancer model using transplanted transformed mouse kidney epithelial cells to nude mice. In their study, autophagosome formation was enhanced preferentially at the center of the tumor mass, which was distant from the vasculature and supposed to be more starved (31). In this study, we detected accumulated autophagosomes in some high-grade tubular adenomas as well as advanced cancers and metastatic lesions. We speculate that cancer cells *in vivo* require autophagy in early stages of tumorigenesis. Once the tumor cells are selected, these cells might maintain the active autophagy. We also assumed that colorectal cancer cells are typical cell types that acquired the higher basal activity of autophagy. We observed that the all tested colorectal cancer–derived cell lines produced comparatively high level of LC3-II protein without induction of autophagy (Fig. 1). The LC3-II protein could not be detected in HeLa cells under the same condition (data not shown).

Taken together, we conclude that active autophagy contributes to tumor cell survival in colorectal cancers *in vitro* and *in vivo*. We also speculate that the pathophysiologic roles of autophagy in tumorigenesis may vary among each type of cancer due to the different biological characteristics of cancer cells and their microenvironments. We would like to extend our investigation to other cancers and clarify the specific regulatory mechanism of autophagy and its relevance to cancer formation and progression.

Acknowledgments

Received 4/19/2007; revised 7/24/2007; accepted 8/10/2007.

Grant support: Ministry of Health, Labour and Welfare for the Third-Term Comprehensive 10-Year Strategy for Cancer Control and Grants-in-Aid for Cancer Research from the Ministry of Health, Labour and Welfare and the Ministry of Education, Science, Sports, and Culture.

The costs of publication of this article were defrayed in part by the payment of page charges. This article must therefore be hereby marked *advertisement* in accordance with 18 U.S.C. Section 1734 solely to indicate this fact.

References

1. Harris AL. Hypoxia—a key regulatory factor in tumour growth. Nat Rev Cancer 2002;2:38–47.
2. Jain RK. Molecular regulation of vessel maturation. Nat Med 2003;9:685–93.
3. Vaupel P, Thews O, Hoeckel M. Treatment resistance of solid tumors: role of hypoxia and anemia. Med Oncol 2001;18:243–59.
4. Kitano M, Kudo M, Maekawa K, et al. Dynamic imaging of pancreatic diseases by contrast enhanced coded phase inversion harmonic ultrasonography. Gut 2004;53:854–9.
5. Esumi H, Izuishi K, Kato K, et al. Hypoxia and nitric oxide treatment confer tolerance to glucose starvation in a 5′-AMP-activated protein kinase-dependent manner. J Biol Chem 2002;277:32791–8.
6. Izuishi K, Kato K, Ogura T, Kinoshita T, Esumi H. Remarkable tolerance of tumor cells to nutrient deprivation: possible new biochemical target for cancer therapy. Cancer Res 2000;60:6201–7.
7. Levine B, Klionsky DJ. Development by self-digestion: molecular mechanisms and biological functions of autophagy. Dev Cell 2004;6:463–77.
8. Tanida I, Tanida-Miyake E, Ueno T, Kominami E. The human homolog of *Saccharomyces cerevisiae* Apg7p is a protein-activating enzyme for multiple substrates including human Apg12p, GATE-16, GABARAP, and MAP-LC3. J Biol Chem 2001;276:1701–6.
9. Tanida I, Minematsu-Ikeguchi N, Ueno T, Kominami E. Lysosomal turnover, but not a cellular level, of endogenous LC3 is a marker for autophagy. Autophagy 2005;1:84–91.

10. Jager S, Bucci C, Tanida I, et al. Role for Rab7 in maturation of late autophagic vacuoles. J Cell Sci 2004; 117:4837–48.
11. Suzuki A, Kusakai G, Kishimoto A, Lu J, Ogura T, Esumi H. ARK5 suppresses the cell death induced by nutrient starvation and death receptors via inhibition of caspase 8 activation, but not by chemotherapeutic agents or UV irradiation. Oncogene 2003;22: 6177–82.
12. Kirkegaard K, Taylor MP, Jackson WT. Cellular autophagy: surrender, avoidance and subversion by microorganisms. Nat Rev Microbiol 2004;2:301–14.
13. Kondo Y, Kanzawa T, Sawaya R, Kondo S. The role of autophagy in cancer development and response to therapy. Nat Rev Cancer 2005;5:726–34.
14. Rez G, Toth S, Palfia Z. Cellular autophagic capacity is highly increased in azaserine-induced premalignant atypical acinar nodule cells. Carcinogenesis 1999;20: 1893–8.
15. Lee HK, Jones RT, Myers RA, Marzella L. Regulation of protein degradation in normal and transformed human bronchial epithelial cells in culture. Arch Biochem Biophys 1992;296:271–8.
16. Ogier-Denis E, Houri JJ, Bauvy C, Codogno P. Guanine nucleotide exchange on heterotrimeric Gi3 protein controls autophagic sequestration in HT-29 cells. J Biol Chem 1996;271:28593–600.
17. Gunn JM, Clark MG, Knowles SE, Hopgood MF, Ballard FJ. Reduced rates of proteolysis in transformed cells. Nature 1977;266:58–60.
18. Kisen GO, Tessitore L, Costelli P, et al. Reduced autophagic activity in primary rat hepatocellular carcinoma and ascites hepatoma cells. Carcinogenesis 1993;14:2501–5.
19. Aita VM, Liang XH, Murty VV, et al. Cloning and genomic organization of beclin 1, a candidate tumor suppressor gene on chromosome 17q21. Genomics 1999; 59:59–65.
20. Liang XH, Jackson S, Seaman M, et al. Induction of autophagy and inhibition of tumorigenesis by beclin 1. Nature 1999;402:672–6.
21. Shintani T, Klionsky DJ. Autophagy in health and disease: a double-edged sword. Science 2004;306:990–5.
22. Crighton D, Wilkinson S, O'Prey J, et al. DRAM, a p53-induced modulator of autophagy, is critical for apoptosis. Cell 2006;126:121–34.
23. Kabeya Y, Mizushima N, Ueno T, et al. LC3, a mammalian homologue of yeast Apg8p, is localized in autophagosome membranes after processing. EMBO J 2000;19:5720–8.
24. Bampton ET, Goemans CG, Niranjan D, Mizushima N, Tolkovsky AM. The dynamics of autophagy visualized in live cells: from autophagosome formation to fusion with endo/lysosomes. Autophagy 2005;1:23–36.
25. Kuma A, Matsui M, Mizushima N. LC3, an autophagosome marker, can be incorporated into protein aggregates independent of autophagy: caution in the interpretation of LC3 localization. Autophagy 2007;3: 323–8.
26. Boya P, Gonzalez-Polo RA, Casares N, et al. Inhibition of macroautophagy triggers apoptosis. Mol Cell Biol 2005;25:1025–40.
27. Kato K, Ogura T, Kishimoto A, et al. Critical roles of AMP-activated protein kinase in constitutive tolerance of cancer cells to nutrient deprivation and tumor formation. Oncogene 2002;21:6082–90.
28. Suzuki A, Kusakai G, Kishimoto A, et al. IGF-1 phosphorylates AMPK-α subunit in ATM-dependent and LKB1-independent manner. Biochem Biophys Res Commun 2004;324:986–92.
29. Suzuki A, Kusakai G, Shimojo Y, et al. Involvement of transforming growth factor-β1 signaling in hypoxia-induced tolerance to glucose starvation. J Biol Chem 2005;280:31557–63.
30. Meley D, Bauvy C, Houben-Weerts JH, et al. AMP-activated protein kinase and the regulation of autophagic proteolysis. J Biol Chem 2006;281:34870–9.
31. Degenhardt K, Mathew R, Beaudoin B, et al. Autophagy promotes tumor cell survival and restricts necrosis, inflammation, and tumorigenesis. Cancer Cell 2006;10:51–64.

Biosci. Biotechnol. Biochem., 71 (4), 1036–1043, 2007

A New Proteasome Inhibitor, TP-110, Induces Apoptosis in Human Prostate Cancer PC-3 Cells

Isao MOMOSE,† Masatomi IIJIMA, Manabu KAWADA, and Daishiro IKEDA

Numazu Bio-Medical Research Institute, Microbial Chemistry Research Center, 18-24 Miyamoto, Numazu, Shizuoka 410-0301, Japan

Received December 13, 2006; Accepted January 13, 2007; Online Publication, April 7, 2007
[doi:10.1271/bbb.60697]

Proteasome inhibitors are useful in the treatment of cancer. Recently, we found a new proteasome inhibitor, TP-110, derived from tyropeptin A produced by *Kitasatospora* sp. Here we report that TP-110 induces apoptosis in human prostate cancer PC-3 cells. TP-110 showed strong cytotoxicity to PC-3 cells (IC_{50} = 0.05 μM). It increased the number of cells in the G_2-M phase and increased the accumulated amounts of the p21 and p27 proteins, which are negative regulators of cell cycle progression. Furthermore, it induced apoptosis along with chromatin condensation and DNA fragmentation in PC-3 cells, and TP-110-induced apoptosis appeared to be associated with caspase activation. Additionally, TP-110 inhibited not only the degradation of IκB and the nuclear translocation of nuclear factor-κB (NF-κB), but also the DNA binding activity of NF-κB. These results indicate that TP-110 shows a strong growth inhibition and apoptosis in PC-3 cells.

Key words: proteasome inhibitor; apoptosis; TP-110

Proteasome is an abundant multi-enzyme complex that provides the main pathway for the degradation of intracellular proteins in eukaryotic cells.[1,2] It degrades numerous regulatory proteins, such as cyclins, cyclin-dependent kinase inhibitors (*e.g.*, p21 and p27), tumor suppressors (*e.g.*, p53), and inhibitory proteins of NF-κB activation (*e.g.*, IκB-α), all of which are critical for tumor growth.[3–6] Proteasome inhibitors can stabilize these regulatory proteins and cause cell cycle arrest and apoptosis, and, as a result, can limit tumor development. Bortezomib (Velcade™), a dipeptide boronic acid proteasome inhibitor,[7,8] has been approved for the treatment of relapsed/refractory multiple myeloma. Therefore, the proteasome inhibitor might be useful in the treatment of various kinds of cancer.[9]

We have found a new proteasome inhibitor, tyropeptin A, which is produced by *Kitasatospora* sp. MK993-dF2.[10–12] Tyropeptin A specifically inhibited the chymotrypsin-like activity of 20S proteasome. We constructed a structural model of tyropeptin A bound to the site responsible for the chymotrypsin-like activity of the mammalian 20S proteasome. Based on these modeling experiments, we designed and synthesized several derivatives of tyropeptin A to enhance its inhibitory potency. Among these, TP-110 strongly inhibited the chymotrypsin-like activity of the 20S proteasome and the growth of various cell lines *in vitro*.[13,14] In the present study, we report that TP-110 induces apoptosis in human prostate cancer PC-3 cells.

Materials and Methods

Antibodies. The antibodies used in Western blotting were as follows: anti-p21 (sc-397), anti-p27 (sc-528), anti-Bax (sc-493), anti-Bcl-2 (sc-492), anti-C23 (sc-13057), anti-NF-κB p65 (sc-109) and anti-NF-κB p50 (sc-8414), from Santa Cruz Biotechnology (Santa Cruz, CA); anti-α-tubulin (T5168) from Sigma-Aldrich (St. Louis, MO); anti-XIAP (AF822) from R&D Systems (Minneapolis, MN); anti-Bcl-X_L (B22630) from Transduction Laboratories (Lexington, KY); and anti-poly (ADP-ribose) polymerase (PARP) (611038) from BD Biosciences (San Jose, CA).

Cells. Human prostate cancer PC-3 cells were obtained from the American Type Culture Collection (Rockville, MD). They were grown in Dulbecco's modified Eagle medium supplemented with 10% fetal bovine serum (Tissue Culture Biologicals, Tulare, CA), 100 U/ml of penicillin G, and 100 μg/ml of streptomycin at 37 °C with 5% CO_2.

Cell growth. The PC-3 cells were cultured in 96-well plates at 5,000 cells/well with a test sample for various times. Cell growth was determined by the 3-(4,5-

† To whom correspondence should be addressed. Fax: +81-55-922-6888; E-mail: imomose@bikaken.or.jp

Abbreviations: NF-κB, nuclear factor-κB; PARP, poly (ADP-ribose) polymerase; MTT, 3-(4,5-dimethyl-2-thiazolyl)-2,5-diphenyl-2H-tetrazolium bromide; RT-PCR, reverse transcription-polymerase chain reaction; GAPDH, glyceraldehyde-3-phosphate dehydrogenase; PCR, polymerase chain reaction; TNF-α, tumor necrosis factor-α

dimethyl-2-thiazolyl)-2,5-diphenyl-2*H*-tetrazolium bromide (MTT) method.[15]

Preparation of cell lysate and Western blotting. PC-3 cells (2×10^5) were cultured in 35-mm dishes with or without TP-110 or MG132 for various durations. The cells were washed twice with ice-cold phosphate-buffered saline containing 100 μM Na_3VO_4 and then lysed in a lysis buffer (20 mM *N*-2-hydroxyethylpiperazine-*N'*-2-ethanesulfonic acid, 150 mM NaCl, 1% Triton X-100, 10% glycerol, 1 mM EDTA, 50 mM NaF, 50 mM β-glycerolphosphate, 1 mM Na_3VO_4, pH 7.5, and 25 μg/ml each of antipain, leupeptin, and pepstatin). Equal protein extracts were separated by SDS–polyacrylamide gel electrophoresis, transferred onto Immobilon polyvinylidene difluoride membranes (Millipore, Bedford, MA) and Western-blotted with anti-p21, anti-p27, anti-Bax, anti-Bcl-2, anti-Bcl-X_L, anti-XIAP, anti-PARP, or anti-tubulin antibodies. Horseradish peroxidase-linked anti-rabbit IgG or anti-mouse IgG antibodies were used as the secondary antibodies (GE Healthcare, Piscataway, NJ). The blots were developed with ECL reagent according to the manufacturer's instructions (GE Healthcare).

Reverse transcription-polymerase chain reaction (RT-PCR) analysis. The PC-3 cells (2×10^5) were cultured in 35-mm dishes with or without the indicated concentrations of TP-110 for 24 h, and then total RNA was isolated using the RNeasy Mini Kit (Qiagen, Valencia, CA). cDNA was synthesized using AMV reverse transcriptase (Promega, Madison, WI) with an equal quantity of total RNA, and amplified using Taq DNA polymerase (Promega). Specific primers of p21, p27, and glyceraldehyde-3-phosphate dehydrogenase (GAPDH) were reported elsewhere.[16,17] The polymerase chain reaction (PCR) was optimized for each set of primers and performed using a different number of cycles to ensure that amplification occurred in a linear range. After amplification, the products were electrophoresed in a 2% agarose gel and then detected by SYBR green I nucleic acid gel staining (Molecular Probes, Eugene, OR).

DNA fragmentation. PC-3 cells (5×10^5) were cultured in 10-cm dishes with TP-110 for 14 or 24 h, and then the cells were washed with phosphate-buffered saline and lysed in lysis buffer containing 0.5% Triton X-100, 10 mM Tris–HCl (pH 7.4), and 10 mM EDTA at room temperature for 10 min. The supernatant fractions, collected by centrifugation at 15,000 rpm for 10 min, were treated with RNase A at 37 °C for 1 h and then treated with Proteinase K (Invitrogen, Carlsbad, CA). The DNA in these fractions was precipitated overnight with NaCl and 2-isopropanol at −20 °C. The DNA was dissolved in 10 mM Tris–HCl (pH 7.4) and 1 mM EDTA buffer, and then separated on a 1.2% agarose gel.

Cell cycle analysis. PC-3 cells (5×10^5) were cultured in 10-cm dishes with or without 0.16 μM TP-110 for 24 h. The harvested cells were fixed with ice-cold 70% ethanol. The fixed cells were then treated with 0.1% RNase A (Sigma-Aldrich) at 37 °C for 15 min, and resuspended in phosphate-buffered saline containing 50 μg/ml propidium iodide (Sigma-Aldrich). DNA fluorescence was measured using a flow cytometer (FACSCalibur, BD Biosciences).

Hoechst 33342 staining. The PC-3 cells (1×10^5) were cultured in 35-mm dishes with or without 0.16 μM TP-110 for 24 h and then stained with 5 μg/ml Hoechst 33342 for 90 min. The nuclear morphology of the cells was visualized using a fluorescence microscope (Leica DM, IRB, Leica Microsystems Wetzlar GmbH, Wetzlar, Germany).

NF-κB activation. The PC-3 cells (2×10^5) were cultured in 35-mm dishes with 1.6 μM TP-110 for 2.5 h before stimulation with 20 ng/ml tumor necrosis factor-α (TNF-α) (R&D Systems). Cytosolic and nuclear fractions were prepared using the cytosol/nuclear fractionation kit (BioVision, Mountain View, CA). Equal protein extracts were analyzed by Western blotting. The DNA-binding activity of NF-κB was quantified using the TransAM NF-κB p65 transcription factor assay kit (Active Motif North America, Carlsbad, CA) according to the manufacturer's instructions.

Statistical analysis. All data are representative of three independent experiments with similar results. The statistical data are expressed as mean ± SD using descriptive statistics.

Results

TP-110 inhibits PC-3 cell growth

TP-110 is a new proteasome inhibitor derived from tyropeptin A isolated from actinomycete (Fig. 1A). In particular, TP-110 selectively inhibited the chymotrypsin-like activity of 20S proteasome and prevented the growth of various cancer cell lines (13). The chymotrypsin-like activity of proteasome in human prostate cancer PC-3 was inhibited 56% by 0.1 μg/ml of TP-110, but it is unclear whether TP-110 induces apoptosis in the cancer cells. Hence we examined the effect of TP-110 on the growth of human prostate cancer PC-3 cells (Fig. 1B). The PC-3 cells were grown with different concentrations of TP-110 for 1 d after TP-110 treatment. On day 2, high concentrations of TP-110 (0.1 and 0.4 μM) decreased the cell density. A medium concentration (0.025 μM) maintained the starting density of the cells and a low concentration (0.0063 μM) did not affect cell growth. The effect of TP-110 on the growth of PC-3 cells was similar to that of MG-132. Next we evaluated the effect of TP-110 on cell viability cultured for 72 h using MTT methods (Fig. 1C). TP-110 strongly inhib-

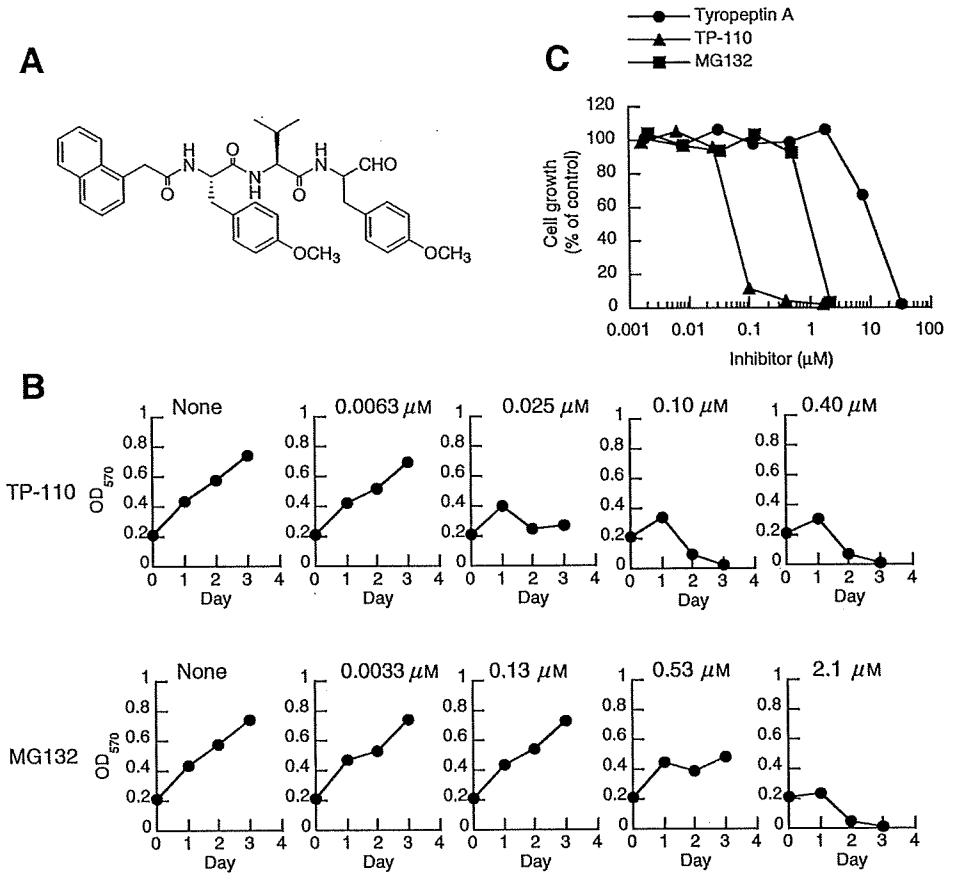

Fig. 1. Effect of TP-110 on PC-3 Cell Growth.

A, Structures of TP-110. B, Growth inhibition by TP-110 on PC-3 cells. PC-3 cells were cultured with the indicated concentrations of TP-110 or MG132 for the indicated times. Cell growth was determined using MTT. C, Cytotoxicity of TP-110 on PC-3 cells. The PC-3 cells were cultured with TP-110, tyropeptin A, or MG132 for 72 h.

ited the growth of the PC-3 cells, and the 50% growth inhibitory concentration (IC_{50}) was determined to be 0.05 μM.

Numerous proteins, including the cyclin-dependent kinase inhibitors p21 and p27, control the cell cycle progression. To examine the potent mechanism of TP-110-induced cell growth inhibition, we evaluated the effect of TP-110 on the protein levels of p21 and p27 in PC-3 cells (Fig. 2A). Accumulation of the p21 and p27 proteins were detected at 8 h after 0.16 μM TP-110 treatment. Next we examined the effect of the various concentrations of TP-110 (Fig. 2B). Although only a trace of p21 protein was detected in the untreated cells, treatment with 0.16 μM TP-110 significantly increased p21 protein at 12 h. p27 protein also increased with 0.16 μM TP-110. Expression of p21 and p27 on the mRNA levels was detected by RT-PCR (Fig. 2C). The expression of p21 was noticeably increased with 0.16 μM TP-110, but p27 did not increase even with 1.6 μM TP-110. Next we evaluated the effect of TP-110 on the cell cycle progression (Fig. 2D). The ability of TP-110 to inhibit cell cycle progression was determined by a combination of propidium iodide staining and the flow cytometer analysis. Treatment of the PC-3 cells with 0.16 μM TP-110 for 12 h resulted in an accumulation of cells in the G_2-M phase along with a decrease in the number of cells in the G_1 phase. Taken together, these results clearly indicate that TP-110 affects proteins that control cell cycle progression, and inhibits cell cycle progression and cell growth.

TP-110 induces apoptosis in PC-3 cells

To investigate whether TP-110 induces apoptosis in PC-3 cells, we examined the apoptotic morphological changes in the PC-3 cells with TP-110. The PC-3 cells were cultured with 0.16 μM TP-110 for 24 h and then stained with Hoechst 33342 (Fig. 3A). TP-110 induced chromatin condensation, which is characteristic of apoptotic cells. To confirm this result, we performed agarose gel electrophoresis of the genomic DNA purified from PC-3 cells cultured with the indicated concentrations of TP-110 for 14 and 24 h (Fig. 3B). TP-110 caused remarkable DNA fragmentation at 0.16 μM TP-110 during a 24 h treatment. To investigate the possible involvement of caspase activation in TP-110-induced apoptosis, we examined the effect of the pan-caspase inhibitor Z-VAD-FMK on apoptosis induction by TP-110 (Fig. 3C). The TP-110-induced DNA frag-

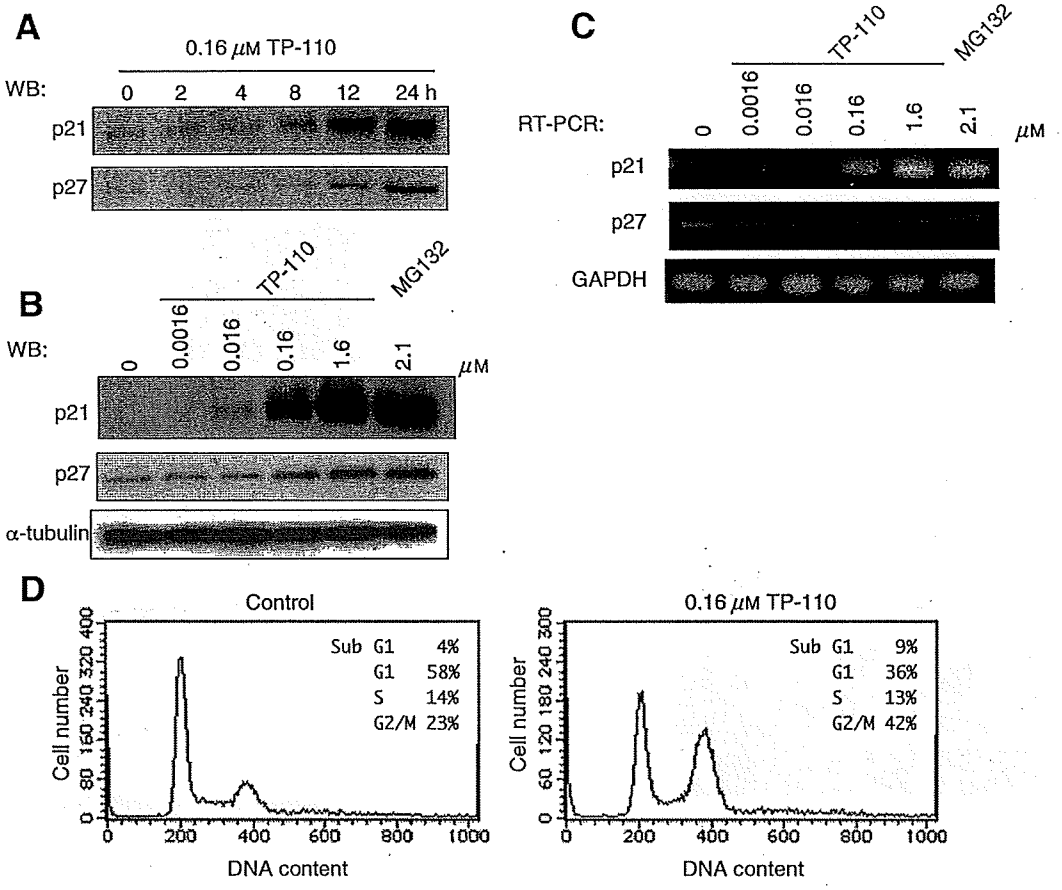

Fig. 2. TP-110 Accumulated p21 and p27 Proteins and Blocked Cell Cycle Progression.

A, Time-dependent accumulation of p21 and p27 proteins by TP-110 treatment. The PC-3 cells were cultured with 0.16 μM TP-110 for the indicated times. Protein extracts were applied to Western blot (WB) using an anti-p21 antibody or an anti-p27 antibody. B, Dose-dependent accumulation of p21 and p27 proteins by TP-110 treatment. PC-3 cells were cultured with the indicated concentrations of TP-110 or MG132 for 12 h. C, The TP-110 induced p21 expression in PC-3 cells. PC-3 cells were cultured with the indicated concentrations of TP-110 or MG132 for 24 h. The p21 and p27 mRNA expressions were assessed by RT-PCR. D, TP-110 blocked cell cycle progression. PC-3 cells were cultured with 0.16 μM of TP-110 for 24 h. The cells were examined by flow cytometer analysis to determine the cell cycle status.

mentations were dose-dependently inhibited by Z-VAD-FMK. Next we evaluated the effect of TP-110 on the protein levels of several apoptosis-related molecules (Fig. 3D). TP-110 decreased the anti-apoptotic proteins Bcl-2 and XIAP, but the anti-apoptotic protein Bcl-X_L did not change. In contrast, the pro-apoptotic protein Bax and the cleaved form of PARP increased. Taken together, these results indicate that TP-110 induces apoptosis in PC-3 cells, and that TP-110-induced apoptosis is dependent on the caspase activation.

TP-110 inhibits TNF-α-stimulated activation of NF-κB in PC-3 cells

The transcription factor NF-κB is involved in cell growth and confers a significant survival potential in a variety of tumors. Proteasome inhibitors, such as bortezomib, are known to inhibit NF-κB activity as one of their diverse actions. To evaluate whether TP-110 inhibits the TNF-α-stimulated activation of NF-κB, we examined the effect of TP-110 on the degradation of the NF-κB inhibitor IκB-α in TNF-α-treated PC-3 cells (Fig. 4A). IκB-α decreased drastically after stimulation of TNF-α in PC-3 cells, but not in TP-110-treated PC-3 cells. Next we examined the effect of TP-110 on the nuclear translocation of the NF-κB p50 and p65 subunits (Fig. 4A). Although TNF-α induced nuclear translocation of the NF-κB p50 and p65 subunits, TP-110 blocked these responses. To confirm the inhibition of NF-κB activation by TP-110 treatment, we further examined whether TP-110 inhibits the DNA-binding activity of NF-κB in PC-3 cells (Fig. 4B). The DNA-binding activity of NF-κB was enhanced by TNF-α, but TP-110 inhibited the DNA-binding activity of NF-κB induced by TNF-α. Taken together, these results indicate that TP-110 inhibits NF-κB activation in PC-3 cells by stabilizing IκB-α.

Discussion

The successful development of bortezomib therapy for the treatment of relapsed/refractory multiple myeloma has proved that proteasome inhibition is an

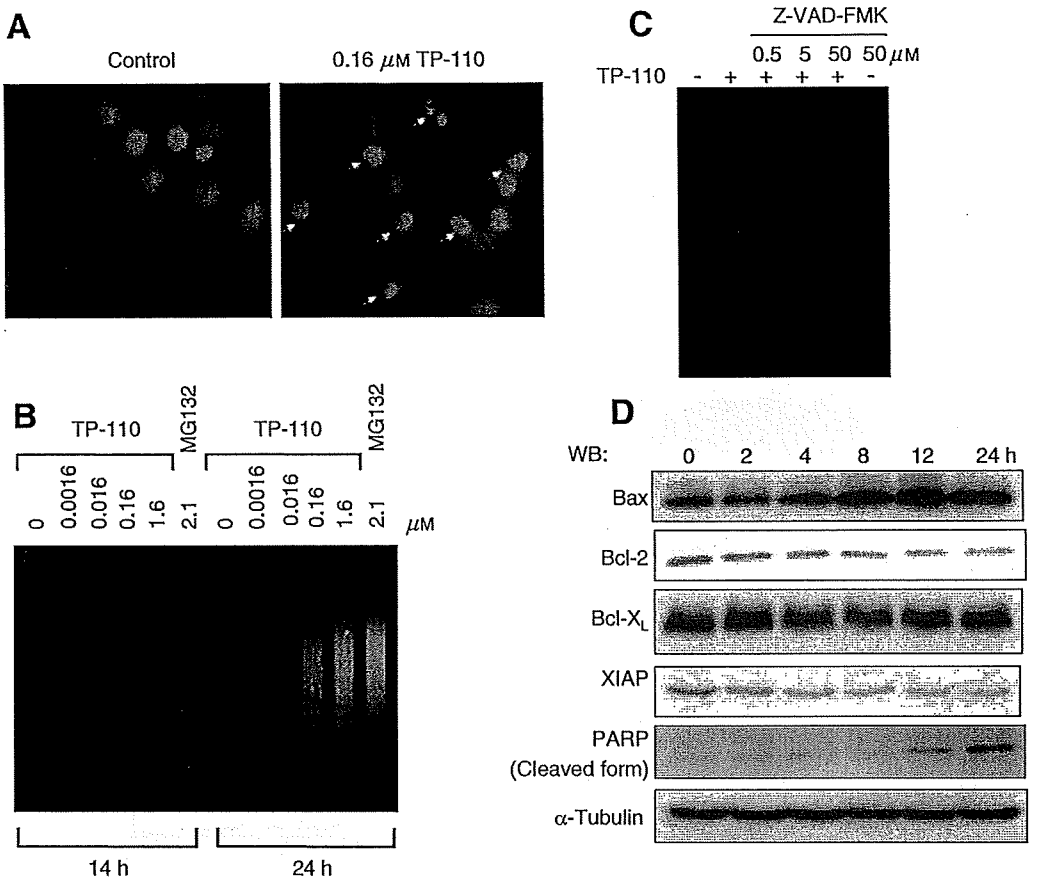

Fig. 3. Induction of Apoptosis by TP-110 in PC-3 Cells.

A, Chromatin condensation by TP-110 treatment. PC-3 cells were cultured with 0.16 μM TP-110 for 24 h, and then the cells were stained with Hoechst 33342. The arrows indicate condensed chromatins. B, DNA fragmentation due to TP-110 treatment. PC-3 cells were cultured with the indicated concentrations of TP-110 or MG132 for 14 or 24 h. Fragmented DNA was isolated and electrophoresed. C, The pan-caspase inhibitor inhibited TP-110-induced DNA fragmentation. PC-3 cells were cultured with 0.16 μM TP-110 and/or the indicated concentrations of the pan-caspase inhibitor Z-VAD-FMK for 24 h. D, The effect of TP-110 on apoptosis-related molecules. PC-3 cells were cultured with 0.16 μM TP-110 for the indicated times. The protein extracts were applied to Western blot analysis.

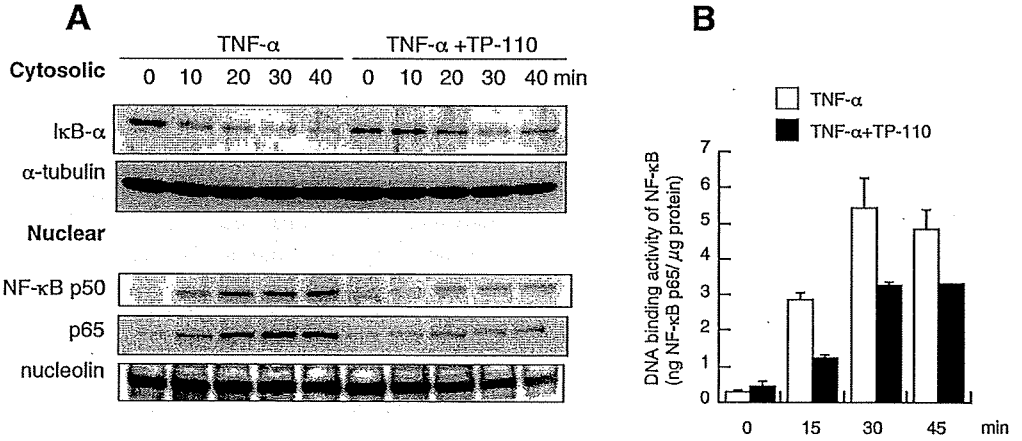

Fig. 4. TP-110 Inhibited TNF-α-Stimulated Activation of NF-κB in PC-3 Cells.

A, TP-110 inhibited TNF-α-stimulated degradation of IκB and nuclear translocation of the NF-κB p50 and p65 subunits. PC-3 cells were precultured with and without 1.6 μM TP-110 for 2.5 h. The cells were further cultured with 20 ng/ml TNF-α for the indicated times. The cytosolic and nuclear fractions were prepared using a Cytosol/Nuclear Fractionation kit. The protein extracts were applied to Western blot analysis. B, TP-110 inhibited the TNF-α-stimulated DNA-binding activity of NF-κB. The DNA-binding activity of NF-κB was quantified using a TransAM NF-κB p65 Transcription Factor Assay kit. Columns, mean of triplicate determinations; bars, SD.

attractive therapeutic strategy, but the prolonged treatment with bortezomib is associated with toxicity and the development of drug resistance.[18] Recent studies have focused on the development of other proteasome inhibitors as therapeutics in cancer tretment. We synthesized a new proteasome inhibitor, TP-110, derived from tyropeptin A produced by *Kitasatospora* sp. MK993-dF2.

First we investigated the effects of TP-110 on the growth of human prostate cancer PC-3 cells (Fig. 1). The PC-3 cells grow with any concentration of TP-110 until 1 d after TP-110 treatment. On day 2, high concentrations of TP-110 were found to decrease cell density. In other words, the cells might make the decision of life or death after the treatment with TP-110 within 1 d. This is supported by the data that 8 h or more were needed to accumulate p21 and p27 proteins under treatment with TP-110 (Fig. 2).

It is known that proteasome degrades p21 and p27.[3,4] The proteasome inhibitor TP-110 was found to inhibit the degradation of p21 and p27 in a time- and dose-dependent manner (Fig. 2). When *de novo* synthesis of the p21 and p27 proteins was inhibited by the protein synthesis inhibitor cycloheximide, the p21 and p27 proteins gradually decreased, but TP-110 suppressed this decrease in the p21 and p27 proteins under cycloheximide treatment (data not shown). Thus it is conceivable that the increase in the p21 and p27 proteins was due to inhibition of the proteasomal degradation of the p21 and p27 proteins by TP-110. But the expression of p21 mRNA was increased by TP-110. Therefore, the increase in p21 protein was due to both inhibition of the proteasomal degradation of p21 protein and to an increase in p21 expression.

Next we evaluated the effect of TP-110 on the cell cycle progression, and found that TP-110 induced an accumulation of cells in the G_2-M phase (Fig. 2). This effect was supported by increased p21 and p27 protein levels, because increased p21 and p27 proteins, in addition to blocking the G_1-S transition, also block the G_2-M transition leading to an accumulation of cells in the G_2-M phase.[19–21] These results clearly indicate that TP-110 affects the proteins that control the cell cycle progression. The expression of p21 mRNA was generally regulated by the p53 protein. However, p53 is null in PC-3 cells,[22] and hence p53 is not required for the TP-110-induced increase in p21 expression in PC-3 cells. Although the mechanism of TP-110-induced p21 expression is not clear, the 3-hydroxy-3-methylglutaryl-coenzyme A (HMG-CoA) reductase inhibitor lovastatin can induce p53-independent transcriptional up-regulation of p21 in human prostate cancer PC-3-M cells.[23] TP-110 might induce p53-independent regulation of p21 as lovastatin dose.

Inhibiting the degradation of the key proteins in cell-cycle regulation causes a disparity in the proliferative signals and eventually leads to apoptosis. Bortezomib and MG132 can arrest cell growth and induce apoptosis. Hence we investigated whether TP-110 can induce apoptosis. As expected, TP-110 induced apoptotic morphological changes with chromatin condensation and caused DNA fragmentation (Fig. 3). Since the TP-110-induced DNA fragmentations were inhibited by the pan-caspase inhibitor, TP-110-induced apoptosis was assumed to be dependent on the caspase pathway. Moreover, TP-110 evoked the cleaved form of the caspase-3 substrate PARP, suggesting caspase-3 activation by TP-110 treatment.

Proteasome inhibitors can overcome NF-κB activation by inhibiting the degradation of IκB.[6,24–26] A major rationale for the therapeutic use of bortezomib is its ability to inhibit NF-κB activation.[27–29] Hence we investigated whether TP-110 inhibits NF-κB activation (Fig. 4). TP-110 inhibited not only the degradation of IκB and the nuclear translocation of the p50 and p65 subunits of NF-κB, but also the DNA-binding activity of NF-κB after TNF-α stimulation, but inhibition of the DNA binding activity of NF-κB by TP-110 was less effective than that of nuclear translocation of NF-κB by TP-110. Phosphorylation of NF-κB p65 stimulates transcriptional activity by promoting an interaction with the coactivator CBP/p300.[30,31] The discrepancy between the degrees of inhibition of nuclear translocation and DNA binding activity of NF-κB can be explained by phosphorylation of NF-κB p65 and coactivator CBP/p300. These results indicate that TP-110 inhibits NF-κB activation in PC-3 cells by stabilizing IκB-α.

Recently, a novel proteasome inhibitor, NPI-0052, was isolated from a new marine actinomycete. It is distinct from bortezomib in its chemical structure and mode of action.[32,33] NPI-0052 was found to inhibit multiple myeloma cell growth *in vivo* and to prolong survival in a murine model. Thus proteasome inhibitors are promising in the therapeutics of cancer. In this study, we found that the proteasome inhibitor TP-110 shows not only cell-growth inhibition, but also induction of apoptosis in PC-3 cells. TP-110 is distinct from bortezomib and MG132 in its chemical structure, and hence it is an attractive lead compound in the treatment of cancer. However, TP-110 unfortunately had only a weak anti-tumor activity *in vivo* (data not shown). The blood concentration of TP-110 rapidly decreased, to half of the initial concentration, within 45 min of intravenous injection. Therefore, TP-110 has poor metabolic stability, and this might limit its anti-tumor activity *in vivo*. We intend to explore tumor cells significantly more sensitive to TP-110 and synthesize more effective and stable TP-110 derivatives.

Acknowledgments

This work was supported by a grant-in-aid for scientific research (no. 15790059) from the Japanese Ministry of Education, Culture, Sports, Science and Technology.

References

1) Coux, O., Tanaka, K., and Goldberg, A. L., Structure and functions of the 20S and 26S proteasomes. *Annu. Rev. Biochem.*, **65**, 801–847 (1996).
2) Voges, D., Zwickl, P., and Baumeister, W., The 26S proteasome: a molecular machine designed for controlled proteolysis. *Annu. Rev. Biochem.*, **68**, 1015–1068 (1996).
3) Maki, C. G., and Howley, P. M., Ubiquitination of p53 and p21 is differentially affected by ionizing and UV radiation. *Mol. Cell. Biol.*, **17**, 355–363 (1997).
4) Pagano, M., Tam, S. W., Theodoras, A. M., Beer-Romero, P., Del, Sal, G., Chau, V., Yew, P. R., Draetta, G. F., and Rolfe, M., Role of the ubiquitin-proteasome pathway in regulating abundance of the cyclin-dependent kinase inhibitor p27. *Science*, **269**, 682–685 (1995).
5) Ciechanover, A., DiGiuseppe, J. A., Bercovich, B., Orian, A., Richter, J. D., Schwartz, A. L., and Brodeur, G. M., Degradation of nuclear oncoproteins by the ubiquitin system *in vitro*. *Proc. Natl. Acad. Sci. USA*, **88**, 139–143 (1991).
6) Palombella, V. J., Rando, O. J., Goldberg, A. L., and Maniatis, T., The ubiquitin-proteasome pathway is required for processing the NF-κB1 precursor protein and the activation of NF-κB. *Cell*, **78**, 773–785 (1994).
7) Adams, J., Behnke, M., Chen, S., Cruickshank, A. A., Dick, L. R., Grenier, L., Klunder, J. M., Ma, Y.-T., Plamonda, L., and Stein, R. L., Potent and selective inhibitors of the proteasome: dipeptidyl boronic acid. *Bioorg. Med. Chem. Lett.*, **8**, 333–338 (1998).
8) Adams, J., Palombella, V. J., Sausville, E. A., Johnson, J., Destree, A., Lazarus, D. D., Maas, J., Pien, C. S., Prakash, S., and Elliott, P. J., Proteasome inhibitors: a novel class of potent and effective antitumor agents. *Cancer Res.*, **59**, 2615–2622 (1999).
9) Adams, J., The proteasome: a suitable antineoplastic target. *Nat. Rev. Cancer*, **4**, 349–360 (2004).
10) Momose, I., Sekizawa, R., Hashizume, H., Kinoshita, N., Homma, Y., Hamada, M., Iinuma, H., and Takeuchi, T., Tyropeptins A and B, new proteasome inhibitors produced by *Kitasatospora* sp. MK993-dF2. I. Taxonomy, isolation, physico-chemical properties and biological activities. *J. Antibiotics*, **54**, 997–1003 (2001).
11) Momose, I., Sekizawa, R., Hirosawa, S., Ikeda, D., Naganawa, H., Iinuma, H., and Takeuchi, T., Tyropeptins A and B, new proteasome inhibitors produced by *Kitasatospora* sp. MK993-dF2. II. Structure determination and synthesis. *J. Antibiotics*, **54**, 1004–1012 (2001).
12) Momose, I., Sekizawa, R., Iinuma, H., and Takeuchi, T., Inhibition of proteasome activity by tyropeptin A in PC12 cells. *Biosci. Biotechnol. Biochem.*, **66**, 2256–2258 (2002).
13) Momose, I., Umezawa, Y., Hirosawa, S., Iinuma, H., and Ikeda, D., Structure-based design of derivatives of tyropeptin A as the potent and selective inhibitors of mammalian 20S proteasome. *Bioorg. Med. Chem. Lett.*, **15**, 1867–1871 (2005).
14) Momose, I., Umezawa, Y., Hirosawa, S., Iijima, M., Iinuma, H., and Ikeda, D., Synthesis and activity of tyropeptin A derivatives as potent and selective inhibitors of mammalian 20S proteasome. *Biosci. Biotechnol. Biochem.*, **69**, 1733–1742 (2005).
15) Mosmann, T., Rapid colorimetric assay for cellular growth and survival: application to proliferation and cytotoxicity assays. *J. Immunol. Methods*, **65**, 55–63 (1983).
16) Kawada, M., Usami, I., Ohba, S., Someno, T., Kim, J., Hayakawa, Y., Nose, K., and Ishizuka, M., Hygrolidin induces p21 expression and abrogates cell cycle progression at G1 and S phases. *Biochem. Biophys. Res. Commun.*, **298**, 178–183 (2002).
17) Schonherr, E., Levkau, B., Schaefer, L., Kresse, H., and Walsh, K., Decorin-mediated signal transduction in endothelial cells. *J. Biol. Chem.*, **276**, 40687–40692 (2001).
18) Chauhan, D., Hideshima, T., and Anderson, K. C., Proteasome inhibition in multiple myeloma: therapeutic implication. *Annu. Rev. Pharmacol. Toxicol.*, **45**, 465–476 (2005).
19) Machiels, B. M., Henfling, M. E., Gerards, W. L., Broers, J. L., Bloemendal, H., Ramaekers, F. C., and Schutte, B., Detailed analysis of cell cycle kinetics upon proteasome inhibition. *Cytometry*, **28**, 243–252 (1997).
20) Dulic, V., Stein, G. H., Far, D. F., and Reed, S. I., Nuclear accumulation of p21Cip1 at the onset of mitosis: a role at the G_2/M-phase transition. *Mol. Cell. Biol.*, **18**, 546–571 (1998).
21) Nakayama, K., Nagahama, H., Minamishima, Y., Miyake, S., Ishida, N., Hatakeyama, S., Kitagawa, M., Iemura, S., Natsume, T., and Nakayama, K., Skp2-mediated degradation of p27 regulates progression into mitosis. *Develop. Cell*, **6**, 661–672 (2004).
22) Planchon, S. M., Wuerzberger, S., Frydman, B., Witiak, D. T., Hutson, P., Church, D. R., Wilding, G., and Boothman, D. A., Beta-lapachone-mediated apoptosis in human promyelocytic leukemia (HL-60) and human prostate cancer cells: a p53-independent response. *Cancer Res.*, **55**, 3706–3711 (1995).
23) Lee, S. J., Ha, M. J., Lee, J., Nguyen, P., Choi, Y. H., Pirnia, F., Kang, W. K., Wang, X. F., Kim, S. J., and Trepel, J. B., Inhibition of the 3-hydroxy-3-methylglutaryl-coenzyme A reductase pathway induces p53-independent transcriptional regulation of p21(WAF1/CIP1) in human prostate carcinoma cells. *J. Biol. Chem.*, **273**, 10618–10623 (1998).
24) Van, Antwerp, D. J., Martin, S. J., Kafri, T., Green, D. R., and Verma, I. M., Suppression of TNF-α-induced apoptosis by NF-κB. *Science*, **274**, 787–789 (1996).
25) Beg, A. A., and Baltimore, D., An essential role for NF-κB in preventing TNF-α-induced cell death. *Science*, **274**, 782–784 (1996).
26) Wang, C. Y., Mayo, M. W., and Baldwin, A. S., Jr., TNF-α and cancer therapy-induced apoptosis: potentiation by inhibition of NF-κB. *Science*, **274**, 784–787 (1996).
27) Adams, J., Preclinical and clinical evaluation of proteasome inhibitor PS-341 for the treatment of cancer. *Curr. Opin. Chem. Biol.*, **6**, 493–500 (2002).
28) Hideshima, T., Chauhan, D., Richardson, P., Mitsiades, C., Mitsiades, N., Hayashi, T., Munshi, N., Dang, L., Castro, A., Palombella, V., Adams, J., and Anderson, K. C., NF-κB as a therapeutic target in multiple myeloma. *J. Biol. Chem.*, **277**, 16639–16647 (2002).
29) Russo, S. M., Tepper, J. E., Baldwin, A. S., Jr., Liu, R., Adams, J., Elliott, P., and Cusack, J. C., Jr., Enhance-